

# RECONSTRUCTING THE DUST CYCLE IN DEEP TIME: THE CASE OF THE LATE PALEOZOIC ICEHOUSE

GERILYN S. SOREGHAN,<sup>1</sup> NICHOLAS G. HEAVENS,<sup>2</sup> LINDA A. HINNOV,<sup>3</sup>  
SARAH M. ACIEGO,<sup>4</sup> and CARL SIMPSON<sup>5</sup>

<sup>1</sup>School of Geology and Geophysics, University of Oklahoma, 100 E. Boyd Street,  
Norman, OK 73019 USA  
<lsoreg@ou.edu>

<sup>2</sup>Department of Atmospheric and Planetary Sciences, Hampton University, 23 E. Tyler Street,  
Hampton, VA 23669 USA

<sup>3</sup>Department of Atmospheric, Oceanic, and Earth Sciences, George Mason University,  
4400 University Drive, Fairfax, VA 20110 USA

<sup>4</sup>Earth and Environmental Sciences, University of Michigan, 2534 C.C. Little Building,  
1100 N. University Street, Ann Arbor, MI 48109 USA

<sup>5</sup>Department of Paleobiology, National Museum of Natural History, Smithsonian Institution,  
Washington, D.C. 20013-7012 USA

---

**ABSTRACT.**—Atmospheric dust constitutes particles <100 µm, or deposits thereof (continental or marine); dust includes ‘loess,’ defined as continental aeolian silt (4–62.5 µm). Dust is well-known from Earth’s near-time (mostly Quaternary) record, and recognized as a high-fidelity archive of climate, but remains under-recognized for deep time. Attributes such as thickness, grain size, magnetism, pedogenesis, and provenance of dust form valuable indicators of paleoclimate to constrain models of atmospheric dustiness. Additionally, dust acts as an agent of climate change via both direct and indirect effects on radiative forcing, and on productivity, and thus the biosphere and carbon cycling. Dust from the late Paleozoic of western equatorial Pangea reflects ultimate derivation from orogens (ancestral Rocky Mountains, Central Pangean Mountains), whereas dust from southwestern Pangea (Bolivia) reflects both proximal volcanism and crustal material. Records of dust conducive to cyclostratigraphic analysis, such as data on dust inputs from carbonate sections, or magnetism in paleo-loess, reveal dust cyclicity at Milankovitch timescales, but resolution is compromised if records are too brief, or irregular in interval or magnitude of the attribute being measured. Climate modeling enables identification of the primary regions of dust sourcing in deep time, and impacts of dust on radiative balance and biogeochemistry. Deep-time modeling remains preliminary, but is achievable, and indicates principal dust sources in the Pangean subtropics, with sources increasing during colder climates. Carbon cycle modeling suggests that glacial-phase dust increases stimulated extreme productivity, potentially increasing algal activity and perturbing ecosystem compositions of the late Paleozoic.

---

## INTRODUCTION

Dust and loess have long been recognized as important components of the Cenozoic Earth system. Loess deposits of the late Cenozoic in particular cover a significant proportion of land area today (~10%; Pye, 1987), and are recognized as high-resolution archives of continental climate. The deposits of the Chinese Loess Plateau, which began accumulating as early as 22 Ma (Guo et al.,

2002) form perhaps the best-known example of loess and its paleoclimatic potential. Intensive research on the Quaternary part of these deposits ultimately led to the discovery that the loess-paleosol succession correlates to the marine oxygen-isotope record of Northern Hemisphere glaciation (Kukla, 1987; Kukla et al., 1988) as well as East Asian summer monsoon variability (Heller and Liu, 1982; Maher and Thompson, 1991), confirming the utility of loess as a high-

resolution climate archive. Subsequently, various proxies including: sedimentology; organic, inorganic, and isotope geochemistry; detrital zircon geochronology; magnetism; paleopedology; and paleobiology have been applied to Cenozoic loess deposits worldwide to assess atmospheric circulation and monsoonal variability, continental temperature and precipitation, and abrupt climate change (e.g., Maher and Thompson, 1995; Sun et al., 2006; Muhs et al., 2008; Antoine et al., 2009; Nie et al., 2013). Beyond loess deposits, eolian dust recovered from lacustrine, marine, and glacial systems is similarly considered an excellent climate archive and, increasingly, an agent of climate and biospheric changes owing to the direct and indirect effects of dust on radiative forcing and carbon cycling (e.g., Mahowald et al., 2011).

Although most research on atmospheric dust has focused on the relatively recent (late Cenozoic) record, loess and dust from Earth's deep-time record are now increasingly recognized, especially from the late Paleozoic (e.g., Soreghan et al., 2008). These deposits house enormous untapped potential as direct, high-resolution archives of continental climate, and may have additionally acted as potent agents of climate change. Accordingly, the purpose of this contribution is to highlight the occurrence, recognition, and utility of loess and dust using the example of the Pennsylvanian–Permian dust record. Recognition of the preservation of dust in deep time opens new avenues for research by sedimentologists, geochemists, paleobiologists, and climate modelers into the drivers and recorders of climate through Earth history, and into climatic-biotic interactions yet to be fully realized. This contribution is organized in five parts, reflecting the various sub-disciplines involved in our ongoing NSF-supported Earth-Life-Transitions project: 1) recognition and relevance of dust, 2) approaches to dust provenance, 3) analysis of dust cyclicity, 4) modeling the impact of dust on Earth's climate, and 5) the impact of dust on Earth's biosphere. This contribution includes both review of key concepts related to dust in deep time, and preliminary results of specific research on this topic.

## RECOGNITION AND RELEVANCE OF DUST IN RECENT AND DEEP TIME

### Definition and formation of loess and dust— informed by the Cenozoic record

Pye (1987) defined dust as a suspension of solid particles in a gas, or a deposit of such particles: because these particles travel in suspension, most are  $<100\text{ }\mu\text{m}$ . Loess consists more specifically of continental deposits of eolian silt (generally 4– $62.5\text{ }\mu\text{m}$  for geologists, but extending to  $2\text{ }\mu\text{m}$  for soil scientists) (e.g., Pye, 1987, 1995; Muhs and Bettis, 2003; Muhs, 2013). Some definitions of loess have included more specific attributes, such as color, porosity, or carbonate content; many of these, however, reflect the late Cenozoic bias of loess research. Hence, we prefer the simple definition above, as it transfers more readily to deep-time deposits. Note that grains larger than  $\sim 20\text{ }\mu\text{m}$  typically settle out of the atmosphere quickly, but the finer fraction can persist for long ( $10^3\text{ km}$ ) distances in atmospheric transport. This very fine fraction ( $<10\text{ }\mu\text{m}$ ) constitutes long-range dust, or atmospheric aerosols, and loess commonly contains this size fraction (Pye, 1987; Muhs, 2013).

Loess often has been described as exclusive to the late Cenozoic (Smalley, 1966; Assallay et al., 1998; Muhs and Bettis, 2003). However, no a priori reason exists for an absence of loess and dust deposits in the deep-time record. Actualism dictates that, if dust and eolian silt form and accumulate on the planet today, then, given the right conditions, they should have in the past as well.

Formation of a dust or loess deposit requires 1) fine-particle generation, 2) wind energy and emission potential, and 3) factors that promote trapping and accumulation (Pye, 1987, 1989; Pye and Sherwin, 1999). Generation of loess in particular is commonly tied to generation of quartz silt because quartz is the predominant mineral in loess (Assallay et al., 1998). Glacial grinding has long been viewed as a particularly effective means to produce large volumes of fines (e.g., Smalley, 1966, 1990, 1995; Kuenen, 1969; Assallay et al., 1998; Muhs and Bettis, 2003; Bullard, 2013), owing in part to the spatial association of loess in proximity to formerly glaciated regions, as well as empirical and experimental data on glacial grinding and silt production (e.g., Jefferson et al., 1997; Wright et al., 1998; Kumar et al., 2006; Soreghan et al., 2015). However, loess and ‘loess-like’ sediments as well as dust also occur in regions far removed from glaciated areas, notably the peri-Saharan region (e.g., Yaalon, 1974; Coude-Gassen, 1987;

Muhs and Bettis, 2003; Crouvi et al., 2010). This association indicates that non-glacial processes such as fluvial and eolian saltation and abrasion, as well as salt-, frost- and insolation weathering also generate fines (e.g., Nahon and Trompette, 1982; Pye, 1987; Assallay et al., 1998; Pye and Sherwin, 1999; Wright, 2001; Muhs and Bettis, 2003; Crouvi et al., 2010, 2012). Indeed, the dustiest place on Earth today is the Saharan Bodélé Depression, which supplies not (abiogenic) quartz silt, but diatomaceous aerosols as well as clay agglomerates blown from the region of pluvial Lake Chad (Prospero et al., 2002; Stutt et al., 2005; Washington et al., 2006; Warren et al., 2007).

Once formed, emission and concentration of the fines occur; in many systems (e.g., proglacial and paraglacial regions), rivers form an important role in transporting and concentrating this material (Smalley et al., 2009). These (generally) high-latitude dust source regions are not necessarily arid, but nevertheless source dust owing to minimal vegetative cover, sediment availability, and winds, which combine to produce high dust-emission potential (Arnalds, 2010; Bullard, 2013; Prospero et al., 2012). Even in low-latitude, desert dust-source regions, evidence for ephemeral water (playas, ephemeral streams) is common (Prospero et al., 2002; Sweeney et al., 2011). Emission potential is affected by soil moisture, surface roughness, vegetation density, saltating particles, and surface crusting (Bagnold, 1941; Sweeney et al., 2011; Sweeney and Mason, 2013)

Finally, dust accumulates in traps, ultimately settling within various environments, e.g., as loess (a continental dust deposit), or within lacustrine, marine, glacial (near-time only), and soil environments (Pye, 1987; Muhs, 2013). Water and vegetation form effective traps; hence, semi-arid regions are better traps than hyperarid regions (Goudie, 1983; Pye and Sherwin, 1999), but loess has even been documented in sub-humid and humid regions, stabilized by grassland and forest vegetation (e.g., Gustavson and Holliday, 1999; Nichol and Nichol, 2013); additionally, topography also plays a role in loess accumulation (e.g., Pye, 1987; Mason et al., 1999; Kidron et al., 2014). Vegetation traps for loess were nonexistent prior to the evolution of land plants, and loess trapping by vegetation probably accelerated after the evolution of grasses in the Eocene. For the late Paleozoic (the focus of this contribution), subhumid/semiarid regions would have likely

supported a mix of small shrub-like plants as well as mosses, ferns, and seed-ferns, albeit not in the densities typical of grasslands (see further discussion below; e.g., DiMichele et al., 2009).

Beyond terrestrial traps (loess, ice, soils), ‘subaqueous’ dust (Stuut, 2014) is preserved in marine and lacustrine sediments. Dust has been recovered from Cenozoic marine sediments from regions sufficiently remote that the transport medium must have been eolian (e.g., Sarnthein et al., 1981; Hovan et al., 1989; Rea, 1994; deMenocal et al., 2000; Stuut et al., 2002). Such truly oceanic archives from remote regions are scarce for the pre-Cretaceous deep-time record, owing to the young age of ocean crust, excepting rare examples of obducted assemblages in ophiolite complexes (e.g., Japan Akiyoshi; Patterson et al., 2011). However, marine records can be recovered from epeiric carbonate systems that formed in regions reasonably isolated from fluvio-deltaic siliciclastic influx (e.g., Soreghan, 1992; Sur et al., 2010), and in paleosols for which an “exotic” (eolian) component can be discerned (e.g., Yaalon and Ganor, 1973; Dahms, 1993; Mason and Jacobs, 1998).

### The relevance of dust and loess for paleoclimatic interpretation

Dust deposits are useful because they form both archives and agents of climate and climate change. Indeed, because these are eolian deposits that travel in suspension in the atmosphere, they constitute a direct geologic record of atmospheric circulation and thus archive synoptic-scale climatology (Muhs, 2013). Moreover, although deposition in loess successions in particular is not necessarily continuous (e.g., Muhs et al., 2014), loess nevertheless archives a high (e.g., millennial) temporal resolution rivaling deep-sea and lacustrine records (Porter and An, 1995; Porter, 2001), but bears the advantage of directly recording atmospheric conditions, rather than conditions processed through a subaqueous filter. The vastness of the ocean acts to buffer the effects of climate change, whereas continental strata record the full dynamic range of climate change (Soreghan and Cohen, 2013). For example, the Chinese Loess Plateau records late Cenozoic Northern Hemisphere glaciation at a fidelity matching the deep-sea oxygen isotope record (e.g., Kukla, 1987; Kukla et al., 1988; Sun et al., 1998; An et al., 2001; Sun, 2002).

Attributes that enable paleoclimatic inferences from loess (and, more generally, dust) begin with

recognition of the presence of such deposits, which reflect dust-emission potential in the source region, in addition to thickness, grain size, and source (reflecting wind direction and strength), and paleosol attributes that include composition and magnetic susceptibility. A vast literature exists on the use of such attributes for Quaternary paleoclimatic reconstructions (e.g., Muhs, 2013), but the same attributes can be tapped for the deep-time record as well (e.g., Soreghan et al., 1997, 2002, 2007, 2011; Tramp et al., 2004; Sweet et al., 2013; Foster et al., 2014).

Dust forms an agent of climate change via both direct and indirect effects on radiative forcing, as well as fertilization effects that influence carbon cycling (e.g., Ridgwell, 2002; Mahowald and Kiehl, 2003; Maher et al., 2010; Mahowald et al., 2011; Highwood and Ryder, 2014; Miller et al., 2014). Dust both scatters and absorbs incoming solar and outgoing long-wave radiation and impacts Earth's energy balance locally and globally (e.g., Tegen et al., 1996). Energy balance affects atmospheric circulation, suppressing precipitation in dusty regions (Yoshioka et al., 2007), an effect that has resulted in megadrought intensification (e.g., Cook et al., 2008, 2009, 2013). In addition, dust affects cloud formation by acting as cloud-condensation or ice nuclei (e.g., Rosenfeld et al., 2001; DeMott et al., 2003). The impacts of dust are linear with atmospheric loading, so modeling shows a stronger global response to dust in dustier climates (Mahowald et al., 2006b). Also, mineral aerosols, as a solid alkaline species within a largely gaseous and acidic atmosphere, affect tropospheric photochemistry (e.g., Martin et al., 2003). The greatest atmospheric radiative effects are from the  $<10\mu\text{m}$  (dust) fraction, which is a significant proportion of loess (Mahowald et al., 2006a).

Much research focuses on the biogeochemical aspects of dust, linked to iron. Iron is a limiting nutrient in the oceans and stimulates primary productivity (Martin and Fitzwater, 1989; Martin et al., 1994; Coale et al., 1996; Boyd et al., 2000). Some N-fixing organisms require more iron than others; notably, much N fixation today occurs downwind of dust plumes (e.g., Capone et al., 1997). Proxy data and biogeochemical models show positive dust-productivity links on glacial-interglacial scales in many ocean regions (Kumar et al., 1995; Kohfeld et al., 2005; Moore et al., 2006; Mahowald, 2011).

Intensive research continues on the impacts of

dust on climate for the modern and recent Earth system, but few studies have addressed dust impacts on the Earth System (climate, biosphere) for deep time (Soreghan and Soreghan, 2002; Gabbott et al., 2010).

### **Recognition of loess and dust in deep time: The case of the Pennsylvanian–Permian**

The late Paleozoic Earth is the most recent analog for the icehouse conditions prevailing through the late Cenozoic, marked by repeated, high-magnitude glacial-interglacial climate shifts beginning in the late Mississippian and linked to continental ice sheets in (southern) high-latitude Gondwanaland (e.g., Crowell, 1999; Fielding et al., 2008; Fig. 1). The late Paleozoic thus bears some similarity to late Cenozoic climate, and new data suggest that extreme variations in dust flux occurred on various spatial and temporal scales. Paleo-loess and related facies have been recognized in western tropical Pangea (Soreghan and Soreghan, 2002; Soreghan et al., 2008a). Examples include massive siltstone interpreted as paleo-loess (e.g., Murphy, 1987; Johnson, 1989; Kessler et al., 2001; Mack and Dinterman, 2002; Soreghan et al., 2002a, 2007; Evans and Reed, 2007; Giles et al., 2013; Sweet et al., 2013; Foster et al., 2014) to silty and “dusty” marine units (e.g., Fischer and Sarnthein, 1988; Soreghan, 1992; Carroll, et al., 1998; Soreghan, et al., 2002a; 2007; Sur et al., 2010a), and in paleosol units (Goebel et al., 1989; Soreghan et al., 2002; Tramp et al., 2004). Deposits from western tropical Pangea indicate a substantial increase in preservation of loess and dust around the Pennsylvanian–Permian boundary (Soreghan et al., 2008a), suggesting that atmospheric dust loading during this interval may have been extreme, albeit more data are needed from other regions to test the spatial extent of this signal.

Key sedimentologic attributes favoring a loess or dust origin for these deep-time strata include the following (Johnson, 1989; Soreghan et al., 2008; Sweet et al., 2013; Foster et al., 2014; Figs. 2, 3): 1) a restricted, albeit not necessarily well-sorted grain-size distribution in the loess/dust mode (typically  $<62\mu\text{m}$ ), and commonly fine-skewed; 2) for loess deposits, thick, structureless bedding, with non-erosive contacts, and no evidence for channeling; and 3) common paleosols intercalated through the succession. For dust influx into marine, lacustrine, or soil environments, the ultimate depositional signal is that of the final (subaqueous or pedogenic)

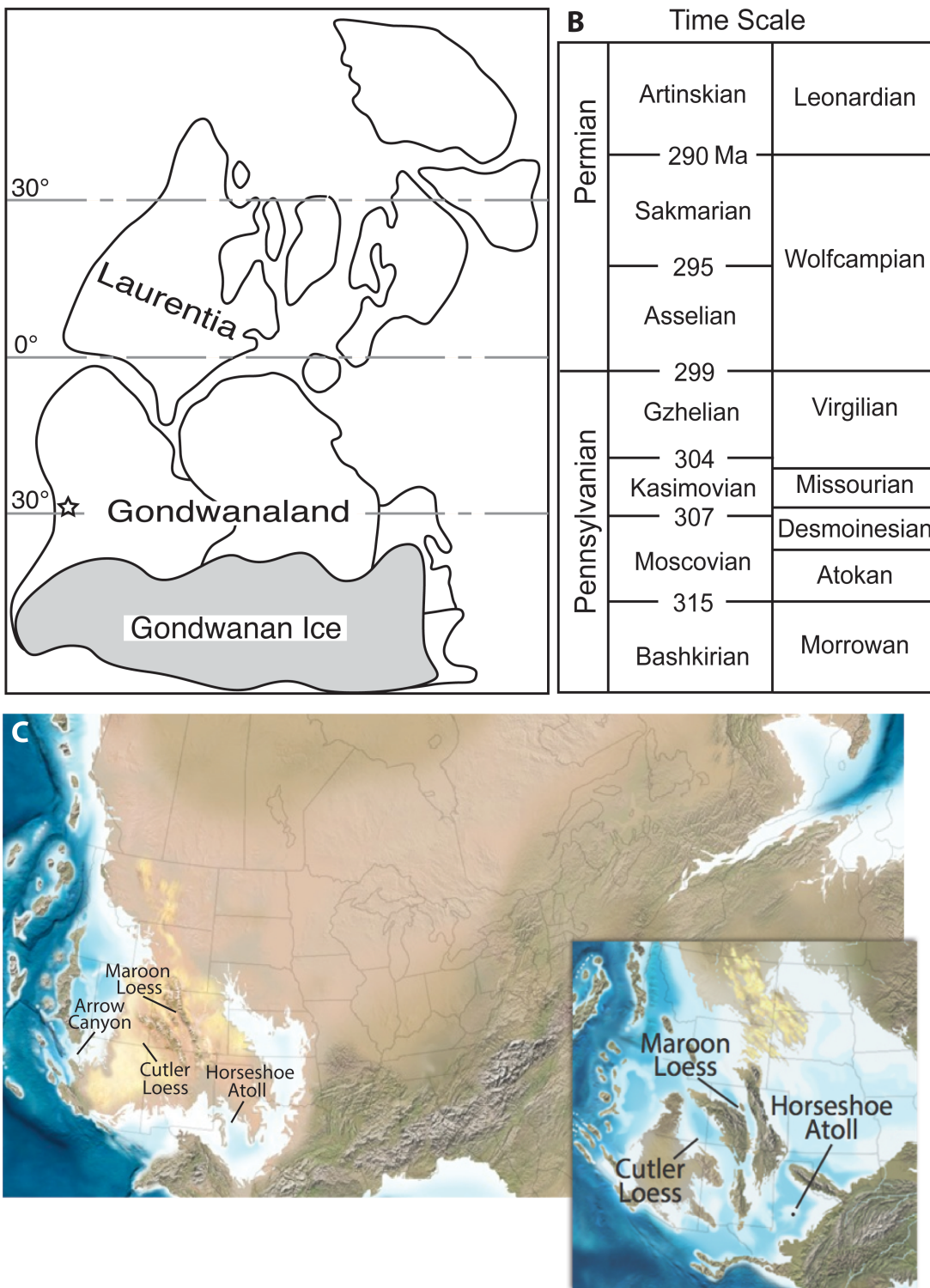


FIGURE 1.—A) Schematic of Pangean paleogeography ~300 Ma. Western North America was located in western equatorial Pangea. Locations of key sections mentioned in the text are noted on (A) and (C). The Akiyoshi (Japan) dust record does not appear on this map; it would plot as a near-equatorial point in the Panthalassic Ocean (far right of the edge of this view). The star indicates the location of the Copacabana Formation (Bolivia). B) Time scale for Pennsylvanian and early Permian time, with international (left) and North American (right) stage names. C) Lowstand glacial and high-stand interglacial (inset) reconstructions for late Paleozoic western equatorial Pangea ~300 Ma (basemap from Blakey, Colorado Plateau Geosystems website).



FIGURE 2.—A) Massive paleo loess of the Permian Flower Pot Shale (Oklahoma). B) Interbedded loess (lighter hue) and paleosols (darker hue) of the Permian Maroon Formation paleoloess (Colorado). C) Core from the Pennsylvanian of the Horseshoe Atoll (West Texas). Most of the interval is carbonate, but dark mudstone occurs at sequence boundaries that records glacial-phase dust influx to this isolated carbonate buildup (Sur et al., 2010). Core is marked in feet (black numbers), and in 10-cm intervals (white bits of paper).

environment; however, evidence for a possible dust contribution includes: 1) a restricted grain size, with an absence of material > silt size, and relatively rare (or subordinate) clay; 2) an allochthonous composition relative to the host strata; 3) an absence of fluvio-deltaic feeder systems (channels), and/or a paleogeographic setting inconsistent with the presence of such systems (e.g., isolated carbonate systems); and 4) a laterally continuous distribution (Soreghan et al., 2002; 2008).

Depending on the diagenetic history of such deposits, data on various attributes can yield paleoclimatically useful information. Many of the same attributes measured from recent loess and dust deposits, such as grain size, provenance, and magnetic attributes, can be extracted from deep-time deposits. For example, grain size is measurable directly from deposits sufficiently friable to be disaggregated using gentle physical and chemical protocols (e.g., Foster et al., 2014; Fig. 3), and 2-D imaging of lithified samples yields relative quartz grain size (Soreghan and

Francus, 2004; M. Soreghan et al., 2015). Provenance can be assessed using primarily geochemical and detrital zircon approaches (see below). Magnetic signals, such as magnetic susceptibility (previously thought restricted to Quaternary loess), are now known to be preserved in deep-time loess as well (Soreghan et al., 1997, 2002; Tramp et al., 2004; M. Soreghan et al., 2015).

## APPROACHES TO DUST PROVENANCE

### Whole-rock geochemistry, detrital zircon geochronology

Owing to its fine-grained character, loess and dust are less amenable to provenance analysis using traditional petrographic point-count approaches typically applied to sand framework composition (e.g., Gazzi-Dickinson method; Ingersoll et al., 1984). This approach can be applied in cases of relatively coarse (e.g., coarse silt mode) loess, but only if the methods are adjusted to accommodate the fine grain size (Soreghan et al., 2008).

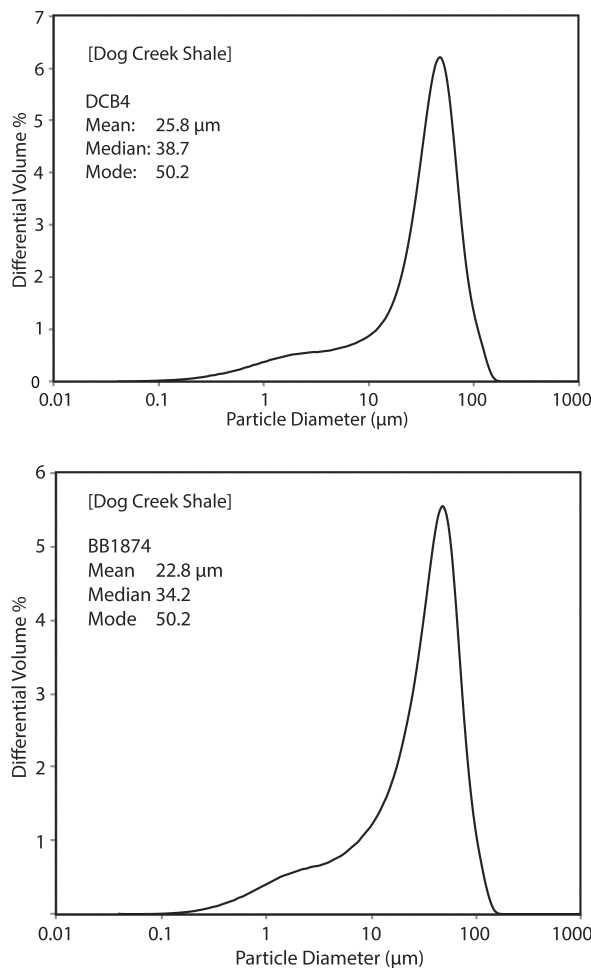


FIGURE 3.—Particle size distributions using laser particle-size analysis on disaggregated loess from the Permian Dog Creek Shale from outcrop in Oklahoma (top) and from core in Kansas (bottom; see Foster et al., 2014).

Accordingly, geochemical and detrital zircon approaches are more effective.

Geochemical approaches that include major/trace/REE compositions have long been applied to fine-grained sediments (overview in Sageman and Lyons, 2004). Ratios of immobile elements, such as Ti/Al and Al/Zr, are thought to track eolian additions to soils (e.g., Mason and Jacobs, 1998); and Th/Sc acts as an index of magmatic differentiation (Taylor and McLennan, 1985), useful for assessing dust provenance (e.g., Gallet et al., 1996), and readily applicable to deep-time deposits (Sur et al., 2010; Sweet et al., 2013; Foster et al., 2014).

Detrital zircon geochronology originated as a provenance tool applied to sandstone units to aid in tectonic reconstructions and “mega” paleogeography/geomorphology (e.g., Riggs et

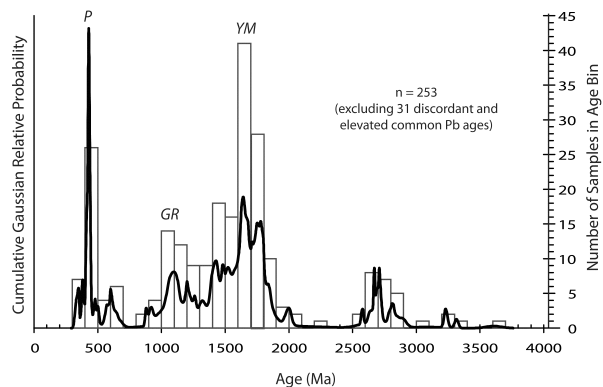


FIGURE 4.—Normalized relative probability plot (black line) and histogram of summed detrital zircon ages from four Pennsylvanian paleo-loess deposits of Arizona and Utah. The relative probability plot depicts the ages and their associated errors, and the histogram depicts the analytical ages (in bins of 100 My). N denotes the number of concordant detrital-zircon ages plotted. P (Paleozoic) and GR (Grenville) peaks are linked to the Central Pangean Mountains and associated terranes, whereas the YM (Yavapai-Mazatzal) peaks reflect erosion of Precambrian basement within the cores of the Ancestral Rocky Mountains uplifts. These sources are common in Pennsylvanian–Permian loess of western equatorial Pangea, with ARM sources more predominant in Pennsylvanian-aged loess, and CPM sources predominant in Permian loess (M. Soreghan et al., 2002, 2014; Soreghan et al., 2007; 2008; 2013).

al., 1996; Rainbird et al., 1997; Gehrels and M. Soreghan, 1998). Advances in instrumentation ultimately enabled analysis of finer grains, leading to application of these approaches to both upper Cenozoic loess (e.g., Aleinikoff et al., 1999, 2008; Stevens et al., 2010; Pullen et al., 2011; Nie et al., 2014) and deep-time loess (M. Soreghan et al., 2002; Soreghan and Soreghan, 2013; Sweet et al., 2013; Foster et al., 2014). These approaches enable reconstruction of transport pathways, which, for the late Paleozoic examples of the western U.S., indicate significant derivation from terranes within the Central Pangean Mountains, with lesser contributions from the Ancestral Rocky Mountains (Fig. 4; references above).

#### Application of radiogenic isotopes to dust provenance

Determining the provenance of dust requires a “fingerprint” of the source that is 1) inherently part of the material; and 2) conservative during deflation, transport, and settling such that the composition remains the same between source and sink areas. While elemental concentrations

and mineralogy may be distinctive of source area, they are grain-size dependent and can fractionate during transport (Grousset and Biscaye, 2005) or during sample processing because of the reagents used for leaching.

Radiogenic isotope tracers are considered robust estimators of source because radiogenic isotopic compositions should not change during transport. Exogenic particles in the atmosphere are either crustal (dust) or mantle (ash) derived, and radiogenic isotopes are significantly different in the mantle versus crust (DePaolo and Wasserburg, 1976; DePaolo, 1980). Furthermore, radiogenic isotopes show variability between crustal source regions based on the age and parent/daughter ratio of the material (Grousset and Biscaye, 2005).

Neodymium isotopes ( $^{143}\text{Nd}/^{144}\text{Nd}$  or  $\epsilon\text{Nd}$ ,  $^{143}\text{Nd}/^{144}\text{Nd}$  normalized to the bulk earth) have been used extensively to resolve source areas with very similar strontium isotope ( $^{87}\text{Sr}/^{86}\text{Sr}$ ) ratios, and the combination of Sr and Nd ratios has been found to be an excellent “fingerprint” in most cases within the recent past (Grousset and Biscaye, 2005). The basis of this fingerprinting is the Sr-Nd isotope plot, where source areas have unique Sr-Nd values due to their different crustal evolution. Figure 5 shows the Sr-Nd composition of modern Northern Hemisphere dust sources. Global dust sources in the Northern Hemisphere that can transport dust via the Arctic are primarily from Asia (data from China/Tibetan Plateau and the Gobi desert/outer Mongolia from Kanayama et al., 2002; Chen et al., 2007).

Hafnium ( $^{176}\text{Hf}/^{177}\text{Hf}$ , or  $\epsilon\text{Hf}$ ,  $^{176}\text{Hf}/^{177}\text{Hf}$  normalized to the bulk Earth composition) may provide additional insight into dust sources and transport. Recently, Lupker et al. (2010) applied Hf isotopes to dust provenance in Greenland ice cores, showing for the first time that at least some of the dust transported to Greenland is not from Asia. The isotopic variability of Hf and Nd in rocks provides a powerful method of identifying the sources of dissolved Hf and Nd in the hydrosphere (Bayon et al., 2009; Rickli et al., 2010). Variable Lu/Hf and Sm/Nd ratios in the minerals will lead to isotopic heterogeneity over time. Therefore, the isotopic composition of the Hf and Nd released during weathering provides constraints on the differential dissolution of various mineral phases: incongruent weathering. The similarity between the Nd isotopic compositions in rivers and the lithologic compositions of their corresponding basins

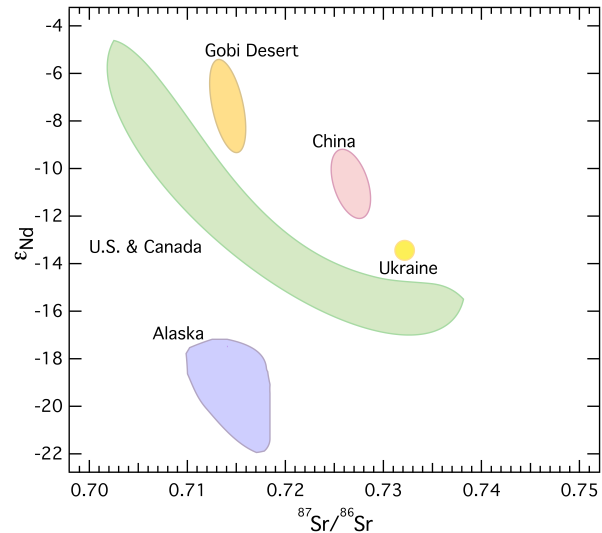


FIGURE 5.—Sr-Nd composition of modern dust from the Northern Hemisphere. Global dust sources in the Northern Hemisphere that can transport dust via the Arctic are primarily from Asia (data from China/Tibetan Plateau and the Gobi desert/outer Mongolia from (Chen et al., 2007; Kanayama et al., 2002).

indicates that Nd is weathered congruently. In contrast to Nd, Hf is not weathered congruently. Early work has shown that as a result of sedimentary sorting, zircons are concentrated in sandy sediments close to continental shelves, which is reflected in low Lu/Hf ratios; and deep sea clays, which are low in zircons, have correspondingly high Lu/Hf ratios. As a consequence of its low Lu/Hf ratio, high resistance to weathering, and density, the retention of unradiogenic Hf in zircons is likely to dominate the observed incongruent weathering of Hf. The differences between the two isotope systems should make them sensitive indicators of both the degree of weathering in the source region, and transport distance due to zircon dominating the variability in dust Hf isotopic composition. In both cases, this is a result of the high density of zircon: the zircon “fall-out” effect changes the isotopic composition of Hf relative to Nd over time/distance (Aarons et al., 2013). Figure 6 illustrates the zircon transport distance and weathering effect: the same source material may have the same Nd isotopic composition but differing Hf composition due to degree of weathering or transport distance.

Very few measurements of Hf in dust have been made to date due to analytical limitations on measuring small samples. However, Rickli et al. (2010) measured ~8 samples, as did Aarons et al.

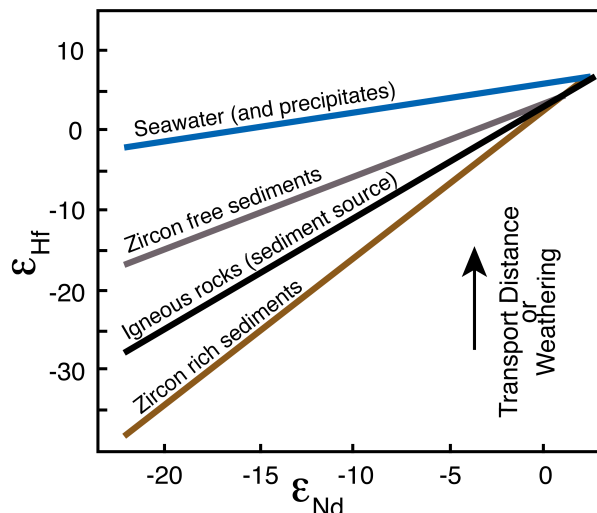


FIGURE 6.—Zircon transport distance and weathering effect: the same source material may have the same Nd isotopic composition but differing Hf composition due to degree of weathering or transport distance.

(2013); in both cases, Hf isotopic compositions were sufficiently variable to show source differences. Aarons et al. (2013) demonstrated that for dust particles  $>5 \mu\text{m}$ , the “zircon effect” should be evident in dust inputs to seawater, ice sheets, and glaciers, and the distance between dust source and deposition site can be modeled based on the Hf isotopic composition.

The primary complication in applying isotopic signatures as direct source “fingerprints” in the geologic past comes in determining the radiogenic isotopic composition of the atmospheric material and their sources at any given point in geologic time. This is a twofold problem: first, identifying the potential source areas and their isotopic compositions and second, making an age correction to the radiogenic isotopic compositions of the atmospheric particles and sources to the point in time at which the particles were incorporated into the sedimentary record.

#### Preliminary results from Pennsylvanian carbonate-hosted dust

Preliminary data from two Moscovian (Middle Pennsylvanian) intervals of the Copacabana Formation, Madre de Dios Basin, Bolivia, are presented here. Two 15-m sections representing carbonate inner-platform environments were processed to separate the fine-grained silicate mineral fraction (SMF). Given the proximity to arc volcanism, ash fall and crustal material both contributed to the atmospheric inputs to this

epeiric marine environment. Our goal is to characterize the isotopic composition of the atmospheric inputs, including the endmember composition of the mantle-derived ash, correct the radiogenic compositions to the age of deposition, and compare this to potential source areas to determine provenance.

To isolate the dust component, leaching procedures were utilized, leaving the silicate mineral fraction (SMF; Sur et al., 2010b). Because of the relatively low concentrations of SMF and the desire to produce a high-time resolution record, analytical methods were employed to provide elemental concentrations and Sr, Nd, and Hf isotopic compositions on the same sample.

Previous studies have demonstrated that low-pressure hotplate dissolutions are prone to incomplete digestion of zircon (Mahlen et al., 2008). Due to the large concentrations of Hf in zircon and low Lu/Hf ratios, incomplete digestion will yield spurious Hf isotopic compositions. Therefore, following previous studies (Patchett and Tatsumoto, 1980; Blichert-Toft et al., 2004; Lapan et al., 2004; Mahlen et al., 2008), a dissolution method capable of breaking down the refractory phases was selected: pressurized, steel-jacketed Parr bombs using a two-phase acid attack.

Approximately 10 mg of sediment were weighed and digested in concentrated Hf using Parr bombs, and these were placed in a 220°C oven for 48 hours. The solutions were carefully desiccated and the procedure replicated with 6 M HCl at 180°C for 12–16 hours. After the final desiccation, 1 mL of 9 M HCl was added for column chemistry. Solutions were then split for elemental analysis by ICPMS, and for ion exchange chromatography and subsequent radiogenic isotope analysis. Elemental concentrations of Rb, Sr, Sm, Nd, Lu, Hf, Fe, and Ti were measured on the Element 2 ICPMS in the Keck Laboratory at the University of Michigan (see Aciego et al., 2015 for measurement description). Ion exchange chromatography was performed following Aciego et al. (2009), providing elemental separation of Sr, Nd, and Hf. Isolated Nd and Sr cuts were measured at the University of Michigan using a Thermo Scientific Triton PLUS Thermal Ionization Mass Spectrometer (TIMS; see Aarons et al., 2013, for measurement description). Isolated Hf cuts were measured at the University of Wyoming using a Thermo Scientific Multi-Collector Neptune PLUS

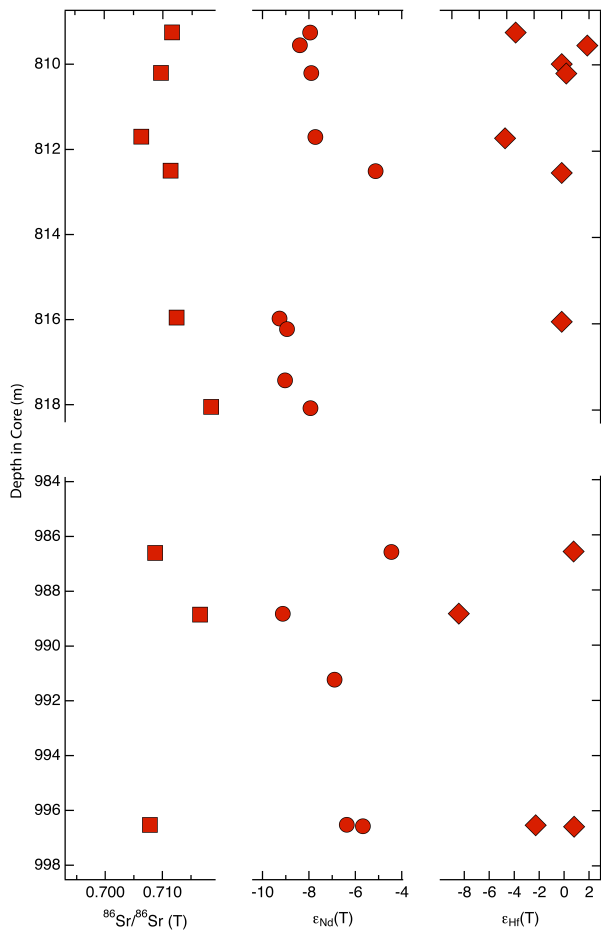


FIGURE 7.—Radiogenic isotope compositions (Sr, Nd, Hf) for preliminary samples from the two intervals, one ash-rich and one ash-poor, of the Moscovian (Pennsylvanian) Copacabana Formation (Bolivia), corrected for depositional age. Strontium indicated with squares, neodymium with circles, and hafnium with diamonds. The ash-rich layers show distinct  $^{143}\text{Nd}/^{144}\text{Nd}$  isotopic compositions ( $\epsilon\text{Nd} = -4.5, 5.7$ ) from the ash poor layers ( $\epsilon\text{Nd} = -6.4$  to  $-9.1$ ). The upper section, free of visible ash layers, exhibits similar  $\epsilon\text{Nd}$  ( $-7.7$  to  $-9.3$  with one outlier at  $-5.1$ ) to the lower section, but more radiogenic  $^{87}\text{Sr}/^{86}\text{Sr}$  compositions ( $0.739$  versus  $0.707$ – $0.717$ ).

ICPMS (MC-ICPMS; see Arendt et al., 2014 for measurement description).

Visual inspection and initial physical-chemical measurements of the dust size fraction indicates discrete differences between the two sections, as well as between ash-rich and ash-poor intervals. The lower section has intervals with up to 72% suspected ash and SMF (non-ash) of 1–7%. The suspected ash layers in the lower section have higher grain sizes (20–40  $\mu\text{m}$ ) compared to the ash-poor intervals (8  $\mu\text{m}$ ). The radiogenic

isotope compositions (Sr, Nd, Hf) were corrected for depositional age and plotted (Fig. 7). Similar to the physical characteristics, the ash-rich layers show  $^{143}\text{Nd}/^{144}\text{Nd}$  isotopic compositions ( $\epsilon\text{Nd} = -4.5$  to  $-5.7$ ) that are distinct from the ash-poor layers ( $\epsilon\text{Nd} = -6.4$  to  $-9.1$ ). The upper section, free of visible ash layers, has high SMF (mean 4–7% up to 41%) with similar size distributions (6–11  $\mu\text{m}$ ) and  $\epsilon\text{Nd}$  ( $-7.7$  to  $-9.3$ , with one outlier at  $-5.1$ , which may indicate potential 'ash' contamination) to the lower section, but more radiogenic  $^{87}\text{Sr}/^{86}\text{Sr}$  compositions (0.73–0.74 versus 0.707–0.717).

Figure 8 shows radiogenic isotopic compositions of the SMF (inferred dust). The ash-rich isotopic compositions plot in a distinctive area of these two-isotope plots, with the crustal-derived (ash-poor) compositions variable and different. However, unlike the modern, there is no isotopic map of the crustal sources for the Pennsylvanian yet, so assigning provenance remains a work in progress. Data mining for Sr, Nd, and Hf radiogenic isotopic compositions of terranes that existed during the Pennsylvanian is the next step in this project. Once potential source areas are identified, Bayesian modeling methods (Arendt et al., 2015) can be applied to determine the relative contributions of ash and dust, as well as different crustal sources of dust.

## ANALYZING DUST CYCLICITY IN DEEP TIME

### Overview

Analysis of the time variations of dust accumulation can elucidate the dynamics of dust generation, transport and deposition. The occurrence of much (albeit not all) late Cenozoic eolian dust has been linked to glaciation and Milankovitch forcing during the Pleistocene Ice Age (An et al., 2014), and we posit the likelihood that dust was affected similarly during the LPIA. Here, a preliminary analysis of dust cyclicity in the Lower Permian paleo-loess of the Maroon Formation, Colorado is presented (Fig. 1; Tramp et al., 2004; Soreghan et al., 2014). One challenge in detecting Milankovitch cycles for the late Paleozoic is that little is known about Earth's astronomical parameters prior to 50 Ma (Laskar et al., 2011a,b). The main issues are discussed further below. Thus it is difficult to anticipate precisely what to look for in cyclostratigraphy to identify Milankovitch forcing. From what is known from dynamics, LPIA stratigraphic cycles

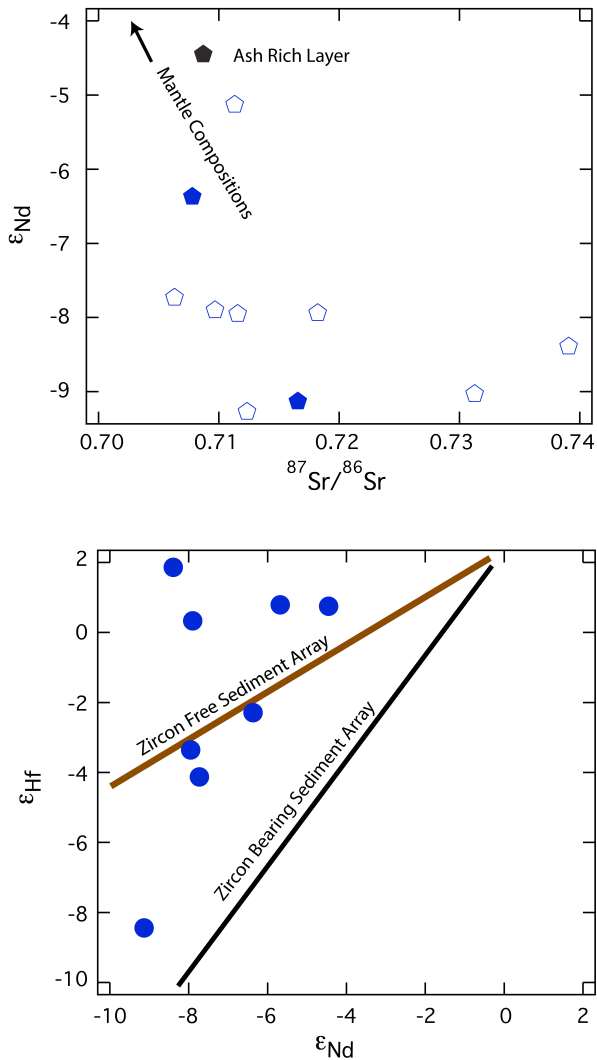


FIGURE 8.—The radiogenic isotopic compositions of the SMF, atmospherically derived material. The ash-rich isotopic compositions plot in a distinctive area of these two-isotope plots, with the crustal-derived (ash poor) compositions variable, and different.

can be expected to be associated with eccentricity, obliquity, and precession in much the same way they are recognized in Cenozoic and Mesozoic-aged stratigraphy (Berger et al., 1992). Another equally serious challenge is geochronology, which is not adequately defined for much of the Paleozoic, including the LPIA. Here, possible Milankovitch-scale cyclicity is assessed using magnetic susceptibility (MS) in the Maroon loessite. We find that the MS series is dominated by precession- and eccentricity-scale variations, suggestive of an equatorial origin for the dust.

#### Modeling Permo–Carboniferous precession, obliquity, and eccentricity.

The challenge for Paleozoic cyclostratigraphy is how to model Milankovitch cycles. The periodicities of the astronomical parameters for the past 10 My are summarized in fig. 4.3 of Hinov and Hilgen (2012). However, significant factors (discussed below) are expected to impose noticeable deep-time impacts on the frequencies of Earth's orbital-rotational parameters.

*Earth's orbital eccentricity and inclination.*—the motions of the planetary orbits are not well constrained for times before 50 Ma owing to three major factors: 1) limited numerical accuracy of the modeling in deep time (Laskar et al., 2004, 2011a,b), 2) evidence for chaotic motions of the planets in deep time (Laskar, 2013), and 3) close encounters with large asteroids (Laskar et al., 2011b). Additionally, (1) frustrates accurate reconstructions of (2) and (3). The expectation is that the Earth's short (130 kyr–95 kyr) orbital eccentricity variations cannot be accurately predicted for times prior to 50 Ma; i.e., the precise zero-crossings and phase change (e.g., La2010a-d as presented in Laskar et al., 2011a; fig. 4). On the other hand, the long 405 kyr orbital eccentricity can be modeled with high accuracy for hundreds of millions of years, with only a one-cycle difference among the Laskar models by 250 Ma (Laskar et al., 2011a; fig. 14). The orbital inclinations of the planets are analogously affected, and are expected to influence Earth's obliquity modulations. However, details of these effects are not known.

*Earth's axial precession rate.*—Earth's axial precession is controlled by the Earth's rotation rate and shape (ellipticity), which are coupled and can also be affected by glacial loading (Thomson, 1990; Bills, 1994; Jiang and Peltier, 1996). While climate forcing is transient, e.g., significant during the ice ages of the past million years, Earth's rotation rate is thought to have been decelerating throughout Earth's history from tidal drag induced primarily by the Moon (e.g., Williams, 2000). Faster rotation rates translate into faster precession rates, higher ellipticity, and shorter obliquity and precessional periods (Berger et al., 1992). For 298 Ma, i.e., the Permo-Carboniferous transition, the periods have been estimated for two models for length-of-day and ellipticity (Berger and Loutre, 1994), and the La2004 astronomical model (Laskar et al., 2004) assumes a different tidal drag model, which can be extrapolated from its end point at 249 Ma to 298 Ma (Yao et al., 2015) for a third estimate (Table 1).

TABLE 1.—Present-day periods for main obliquity, long- and short precession

Parameter	Present day	Model 1 (kyr)	Model 2 (kyr)	La2004 extrapolated (kyr)
Main obliquity	34.291	34.163	31.106	
Long precession	20.725	20.678	19.618	
Short precession	17.421	17.387	16.800	

To summarize, the 405-kyr orbital eccentricity cycle is expected to be present in Milankovitch-forced Carboniferous strata, and recent geochronology suggests that the classic Pennsylvanian cyclothsems are responses to this cycle (Davydov et al., 2010; Schmitz and Davydov, 2012). If the 405-kyr cycle can be identified in cyclostratigraphy, then the periodicities of the obliquity and precession can be determined, provided no hiatuses are present.

#### Dust proxy time-series analysis of the Permian Maroon Formation paleo-loess

A 700 m section of the Maroon Formation paleo-loess comprises meter-scale loessite-paleosol cycles, and magnetic susceptibility (MS) measured along the sequence (Tramp et al., 2004; fig. 5) provides the opportunity to conduct time-series analysis. Young (volcanic) detrital zircons at the top and base of the studied section constrain the age between 297.1 Ma and 288 Ma for a maximum possible duration of 9.1 Myr (M. Soreghan et al., 2014).

The time-series analysis applied here aims to characterize frequencies of dust proxy variations. Power spectral analysis, which partitions variance (“power”) of the dust proxy series as a function of frequency, was used for this analysis. Because the series in this case are recorded as a function of depth and stratigraphic position, the power spectra report spatial frequency (e.g., cycles/meter). The inverse of spatial frequency is wavelength, and spectral peaks at specific wavelengths identify sediment cycle thicknesses. Finally, application of a sedimentation rate converts wavelength to periodicity. The two proxy series are thought to resolve the Milankovitch band, i.e., variations in the  $10^4$ – $10^6$  year range, which requires modeling Milankovitch cycles expected for Permo-

Carboniferous time.

Power spectral analysis was performed with the prolate multitaper method (Thomson, 1982), and classical AR(1) red-noise analysis was applied to identify significant cycles (see description in Kodama and Hinnov, 2015). Bandpass filtering was carried out using the Taner filter (Taner, 2000), with passbands defined by center, upper, and lower cut-off frequencies. LOESS smoothing is computed with weighted linear least-squares fitting to a second-degree polynomial model. These procedures are performed in Matlab (see Appendix in Kodama and Hinnov, 2015).

The longest continuous set of MS measurements from 0–253 m was selected for time-series analysis (Fig. 9), representing  $(253 \text{ m} / 700 \text{ m}) \times 9.1 \text{ Myr} = 3.29 \text{ Myr}$  maximum duration. There are 120 visible loess/paleosol cycles in this interval (averaging 2.12 m thick, median 1.45 m). Each cycle has an  $\sim 3.29 \text{ myr} / 120 = 0.0274 \text{ myr} = 27.4 \text{ kyr}$  maximum duration. Over 398 m of section, there are 170 cycles averaging 2.34 m thickness per cycle, or a  $(398/700) \times 9.1 \text{ myr} = 5.174 \text{ myr}$  maximum duration, and  $5.174 \text{ myr} / 170 = 0.030435 \text{ myr} = 30.435 \text{ kyr}$  per cycle maximum duration. These cycle duration estimates are both shorter than the fastest model of the obliquity (31.106 kyr; Table 1), so if Milankovitch forcing was at play, the dominant forcing mechanism was most likely the precession ( $\sim 20$  kyr long precession and  $\sim 17$  kyr short precession, Table 1).

The Maroon Formation MS series indicates that loessite is represented by relatively low MS values, and paleosols are indicated by high MS values (Tramp et al., 2004). The series has a very low-frequency cycle (wavelength of  $\sim 100$  m to 125 m; Fig. 9A). Its removal improves visualization of the high frequencies and reveals that the basic 1.45 m to 2.12 m loessite-paleosol cycles are “bundled” into lower-frequency cycles (wavelengths of 5 m to 10 m; Fig. 9B). Both basic and bundling cycles are thinner near the center of the succession, where MS values are relatively low. This suggests lower sedimentation rates in this interval (100 m to 150 m). These cycles are borne out in the power spectrum (Fig. 9C), with significant spectral peaks at 1.02 m, 1.4 m, 1.8 m, 6.1 m, and 8.6 m.

If the 1.4 m cycles are representative of 19.618 kyr-long precession (Table 1, La2004 extrapolated model), then the sedimentation rate of the series is  $1.4 \text{ m} / 19.618 \text{ kyr} = 0.071363 \text{ m/kyr}$ .

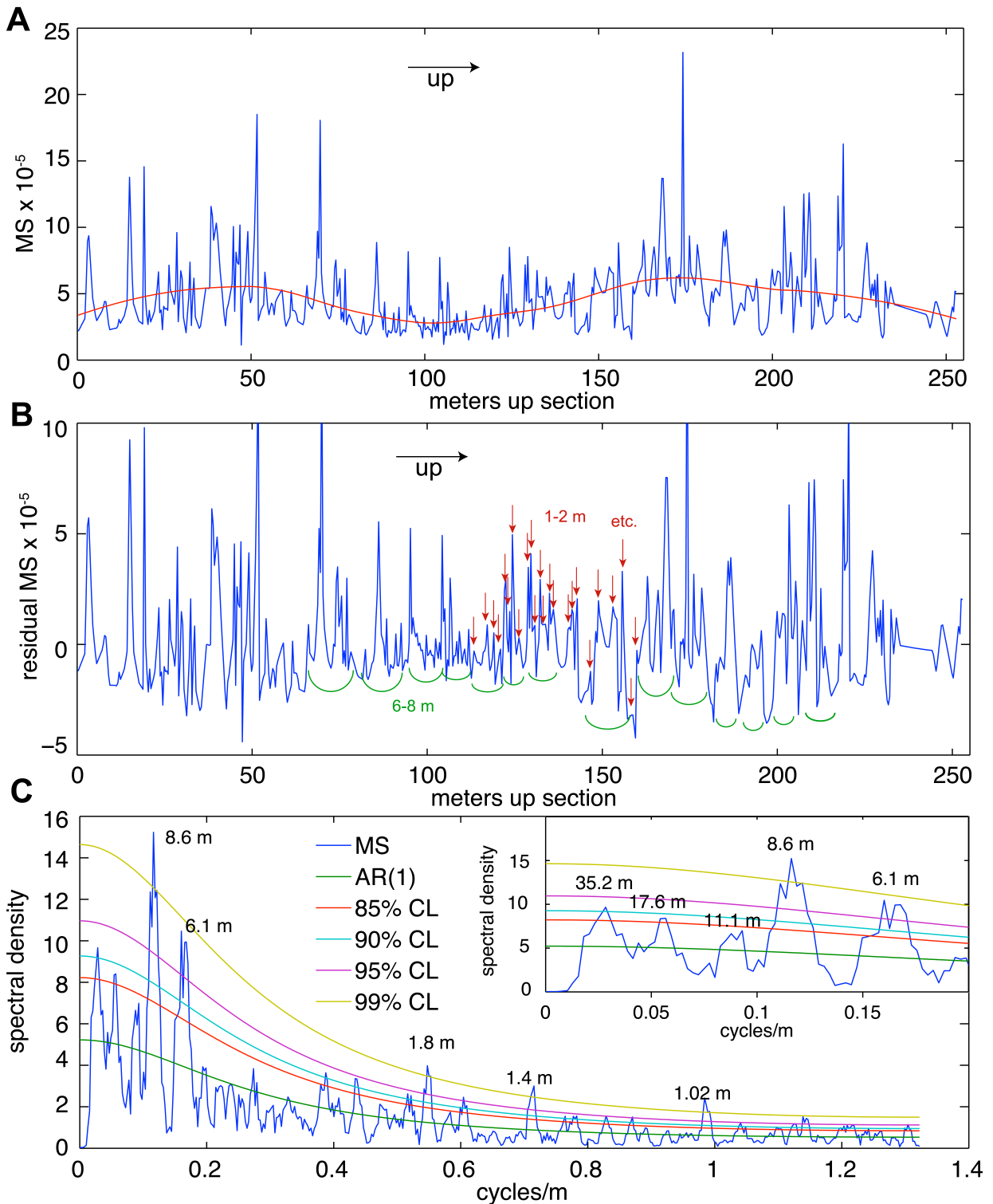


FIGURE 9.—Time-series analysis of the Maroon Formation MS series. A) The original MS series of Tramp et al. (2004), resampled to the mean sample spacing of 0.3781 m. The smooth LOESS curve computed with a 100 m window captures a long cycle of 100 m to 125 m. B) Residual MS series following removal of the LOESS curve in A. Major cycles (identified in C) are demarcated. C)  $2\pi$  MTM power spectrum of the residual MS series (in B); the classical AR(1) red-noise model is shown with confidence levels (CL) from low (85%) to high power (99%). Spectral peaks exceeding 95% CL are labeled with period calibration summarized in Table 2. The 1–2 m cycles are interpreted as precession; the 6–8 m cycles as short eccentricity.

TABLE 2.—Time calibration of significant spectral peaks in Fig. 9C

Wavelength (m)	Model 1 (kyr)	Model 2 (kyr)	La2004 extrapolated (kyr)
1.02	15.100	15.065	14.293
<b>1.4</b>	<b>20.725</b>	<b>20.678</b>	<b>19.618</b>
1.8	26.646	26.586	25.223
6.1	90.302	90.097	85.478
8.6	127.31	127.02	120.51

kyr (close to the average sedimentation rate of 700 m/9100 kyr = 0.0769 m/kyr). This calibrates the 6.1 m cycle to 6.1 m/(0.071363 m/kyr) = 85.5 kyr, and the 8.6 m cycle to 8.6 m/(0.071363 m/kyr) to 120.5 kyr, suggestive of short eccentricity (124 kyr to 131 kyr and 95 kyr to 99 kyr; see Hinnov and Hilgen, 2012, fig. 4.3a). Calibration of the 1.4 m cycles to all three long precession models of Table 1 is summarized in Table 2. There does not appear to be a contribution from obliquity forcing, although the 1.8 m component, which calibrates to ~26 kyr, could be evidence, misaligned by sedimentation rate variations. A 405 kyr-long eccentricity cycle should be present as a  $4 \times 6.1$  m = 24.4 m cycle, but does not appear in the spectrum, unless embedded in the 17.6 m and 35.2 m spectral peaks and masked by sedimentation rate variations (see inset, Fig. 9C). Finally, the 100 m to 125 m cycle has a periodicity of 100 m/(0.071363 m/kyr) = 1402 myr to 125 m/(0.071363 m/kyr) = 1752 myr. This may be the astronomical cycle related to  $g_4-g_3$ , the beat frequency between the orbital perihelia of Mars and Earth, which is 2.4 Myr during the Cenozoic, but is modeled as progressively shorter back through geologic time (Laskar et al., 2011a).

### Cyclostratigraphy of dust in deep time

This analysis is beset with the usual problems that plague the study of ancient cyclostratigraphy:

The Maroon MS series has limited chronostratigraphic constraints provided by a few (inferred) syndepositional detrital zircons. The sample spacing of the proxies of the MS series is not uniform, which requires resampling to the mean spacing in order to estimate the classical red-noise model together with multitaper spectral analysis. Other appropriate spectral estimators for non-uniformly spaced time series should also be

explored (e.g., Schulz and Mudelsee, 2002). Finally, the Maroon series in particular shows signs of strong sedimentation rate variations. This causes an unknown degree of distortion to the power spectrum, which, if corrected, could change the interpretation of the cycles proposed in this study. This enters the controversial realm of tuning, which traditionally has been fraught with subjectivity and circular reasoning. However, objective techniques are being developed that can minimize circularity, e.g., the average spectral misfit method of Meyers and Sageman (2007).

The apparent Milankovitch forcing of the Maroon loessite provides clues about LPIA climatic change. The analyzed cyclicity points to precession forcing of 1–2 m scale loessite-paleosol cycles and a strong bundling of these basic cycles at 5–10 m, which is at the ~100 kyr short eccentricity scale. This contrasts with the glaciation-driven Quaternary middle-latitude Chinese loess cycles, which reflect the strong 100 kyr eccentricity cycles of marine  $\delta^{18}\text{O}$  (for the time since the mid-Pleistocene transition), with strong obliquity forcing prior to the mid Pleistocene (An, 2014). In contrast, precession-eccentricity forcing is characteristic of equatorial regions, and its strong presence (and weak to no obliquity signal) in the MS series suggests an equatorial origin for dust cycling.

## MODELING THE IMPACT OF DUST ON EARTH'S CLIMATE SYSTEM

### Overview

The types of questions posed about the history of the dust cycle in both recent and deep intervals of Earth history center on three aspects of the Earth system: 1) sediment cycling (e.g., What are the largest dust sources on the planet?); 2) the climate system (e.g., What is the impact of dust on radiative balance at the top of the atmosphere?); and 3) biogeochemical cycling (e.g., What is the impact of dust deposition on biological productivity in the ocean?). None of these questions can be answered quantitatively from the geological record alone.

The major obstacle to a purely geological reconstruction in the first example is that deposition sites can be strongly influenced by proximal, but globally insignificant dust sources. In low-latitude Holocene and Pleistocene ice cores from South America, the influence of local topography and variations in sediment availability as local lake levels change produces wide

variability in dust deposition on scales of 1000 km, but these sources are not globally significant (Mahowald et al., 1999). It has been proposed that high deposition rates within 25–50 km of continental interior source areas (e.g., Roberts et al., 2003) also are not globally significant. The argument is the grain-size distribution varies strongly across this (25–50 km) distance, such that depositional rates in the source area fail to correlate strongly with the source area's contribution of fine dust to the global atmosphere (Albani et al., 2015). Any non-uniformity in the spatial coverage of data will lead to biases in quantifying the strength of dust sources. The major obstacle in the second example is that the extant geological information about dust deposition cannot constrain the residence time of dust in the atmosphere or the seasonality of dust transport, both of which are necessary to evaluate its radiative impact. The major obstacle in the third example is again spatial non-uniformity. Especially in deep time, few records of oceanic deposition exist, thwarting extrapolation to the entirety of the global ocean.

To overcome these obstacles when studying the history of the dust cycle during the Holocene and the Pleistocene, global climate models (GCM) have been adapted to synthesize dust deposition records into coherent reconstructions of the dust cycle (Joussaume, 1993; Mahowald et al., 1999, 2006a, 2010; Tegen et al., 2001; Li et al., 2010; Albani et al., 2015). Ideally, these models provide globally complete, spatially uniform accounts of dust lifting, transport, and deposition that are consistent with known physics, and agree with geological records of dust from the interval studied. Depending on the GCM used, these simulations also can quantify the impacts of dust on the climate system and even its biogeochemical impacts in the marine and terrestrial realms (Mahowald et al., 2006b; Okin et al., 2004, 2011).

In the remainder of this section, we describe how a GCM was used to reconstruct dust deposition during the LPIA. The uncertainties in the reconstruction are large, but we propose that a concrete example more vividly illustrates the challenges of applying dust cycle reconstruction techniques developed for more recent intervals to deep time than an abstract review would. Weaknesses and uncertainties in this approach or alternate approaches that could have been used are highlighted as well.

### **Baseline climate simulations for the Late Paleozoic Ice Age**

The first step for dust cycle reconstruction using a GCM is to simulate climate for a specific time interval without explicitly accounting for the radiative impact of dust. These are the baseline climate simulations. To create baseline climate simulations for LPIA conditions, an ensemble of simulations for an Asselian (Early Permian) paleogeography were generated in the Community Climate System Model version 3 (CCSM3; Heavens et al., 2015). Each model simulation was static with respect to key atmospheric and surface boundary conditions such as greenhouse gases, sea level, vegetation distribution, and ice-sheet location and extent. The parameters of the vegetation varied seasonally, but all of the other parameters did not vary over the course of the simulations. Varying boundary conditions one at a time created the ensemble. The simulations then were run until they were in approximate radiative equilibrium and minimally drifting in surface temperature.

One advantage of CCSM3 in particular is that it can utilize parameterizations for simulating dust emission and transport (see Mahowald et al. 2006 for details). Note that dust cycle parameterizations typically include parameterizations of dust emission as well as parameterizations that govern the removal of dust from the atmosphere by wet and dry deposition. The parameterizations that govern dust emission roughly approximate relationships between dust emission, wind, and surface/soil properties established by a wide body of laboratory and field experimentation as well as physical theory (e.g., Marticorena and Bergametti, 1995; Shao et al., 2002). As discussed later in detail, these parameterizations typically attempt to capture reduced dust emission from wet soils but often neglect the similarly inhibiting effects of salt crusts or the mixture of immobile grain sizes with the dust.

For some types of studies, there is no need to use the same model to simulate baseline climate as to simulate the dust cycle. A class of offline dust-transport models exist that adopt necessary information from the baseline climate simulations and simulate the dust cycle based on its output. One good example of such an offline dust transport model is the Mineral Dust Entrainment and Deposition model (DEAD; Zender et al., 2003a). The main demerit of using these models is that feedback effects between dust and model climate cannot be assessed. Nevertheless, offline

models could enable deep-time climate simulations that already exist to be utilized for dust cycle studies.

### Uncertainties in simulating late Paleozoic climates

Generating baseline simulations for deep-time climates presents challenges well beyond those that exist for more recent intervals. For example, boundary conditions for the Last Glacial Maximum (LGM) are well known. Global topography and bathymetry approximate that of the present day, greenhouse gas levels are available from ice-core data (e.g., Anklan et al., 1997), and global sea level can be reconstructed from tectonically undisturbed settings (Lambeck et al., 2014). Moreover, palynology and similar techniques have generated a global dataset of biome distribution for the LGM (Prentice et al., 2000; Harrison et al., 2001; Bigelow et al., 2003; Pickett et al., 2004) that can be validated against an equilibrium vegetation model (BIOME4) to determine biome distribution where data are sparse (Kaplan et al., 2003). In addition, the phenology and transpirative properties of most LGM plants are observable in their modern descendants. Finally, high-resolution reconstructions of ice-sheet extent and thickness exist from sedimentology, exposure-age dating, sea-level histories, and geodesy (e.g., Peltier et al., 2015).

All of these data exist in some form for the LPIA, often in multiple versions. Topography, bathymetry, sea level, and glacial extent can come from integrated paleogeographic reconstructions such as those of Ziegler et al. (1997) or Scotese (2001). Reconstructions of greenhouse gas levels (e.g., Berner and Kothavala, 2001; Montañez et al., 2007), and biome data exist as well (e.g., Rees et al., 2002).

The difference in quality between boundary condition datasets for the LGM and the LPIA is that the uncertainties are much larger, data are sparser, and age control is poorer for the LPIA. Uncertainties in greenhouse gas reconstructions, for example, are so large that Asselian pCO<sub>2</sub> could have ranged from 0–1000 ppmv (Montañez et al., 2007). However, the lower end of the uncertainty range can be excluded here, because low pCO<sub>2</sub> levels impose high physiological stresses in plants, which have not been observed in the early Permian paleobotanical record (Pagani et al., 2009; Gerhart and Ward, 2010).

Data are so sparse that glacial extent

reconstructions are highly sensitive to changes in sedimentological interpretations or estimated paleolatitude. The Unayzah Formation in Saudi Arabia, which moved from 75° S to 28° S between Moscovian and Kungurian time, illustrates this sensitivity well. The area was glaciated in Moscovian–Gzhelian time (when at 75° S) but was certainly deglaciated by the time the area reached 28° S (Melvin et al., 2010), yet reconstructions such as Scotese (2001) show ice sheet advance to 40° S on the basis of earlier paleomagnetic data, suggesting the area was glaciated while at that latitude.

Biome reconstructions are also difficult to apply in climate models where vegetation modules are designed for modern vegetation. These differences probably introduce minimal uncertainty into global surface radiative balance and the hydrological cycle, but may be important locally (Horton et al., 2010; Heavens et al., 2015). In addition, vegetation cover is a major control on dust mobilization and is currently incorporated into models in some form (e.g., Mahowald et al., 1999, 2006a). Plant cover reduces shear stress at the surface, inhibiting the mobilization of dust (Marticorena and Bergametti, 1995; Okin and Gillette, 2001; Okin, 2008). In the modern prairie biome, the deep roots of grasses bind soil together and support retention of precipitation as soil moisture, both of which prevent erosion (Weaver and Harmon, 1935).

Modelers can have little confidence that equilibrium or dynamic vegetation models can predict what biomes are present in the absence of a paleobotanical record, and that modern biome properties are good analogs for the properties of late Paleozoic biomes. For example, Boyce et al. (2009) argued that the physiological structure of angiosperms had evapotranspirative advantages over earlier trees attributable to their much higher leaf vein density. Wilson and Knoll (2010) disputed this, and showed that Paleozoic trees had transpirative properties comparable to modern conifers and angiosperms, even if their modern-day descendants do not.

The paleobotanical records of late Paleozoic tropical forest biomes suggest forest structure once was very different, whatever the physiological differences of the trees. Studies of well-preserved forests from Pennsylvanian strata suggest that tropical forests generally included more open canopies than modern rainforests (DiMichele and Falcon-Lang, 2011). Closed-forest canopies resembling those of modern

forests are thought to have developed during the Cretaceous, when seeds adapted to developing under closed canopies appear in the fossil record (Morley, 2011). At present, the effect of these ancient versus modern biomes uncertainties is thought to introduce minimal uncertainty into aspects of physical climate, such as global surface radiative balance and the hydrological cycle, but may be important for precipitation and radiative balance locally (Horton et al., 2010; Heavens et al., 2015).

Differences between late Paleozoic and ancient biomes may matter more for dust emission than for physical climate. Overpredicting tropical forests could result in underestimating the extent of dust sources. Differences in biome properties would matter more for drier biomes. It appears that vegetation only started colonizing dry alluvial fans in the Pennsylvanian (Falcon-Lang, 2003, 2006; Gibling and Davies, 2012). The earliest fossil evidence for grasses dates to the latest Cretaceous (Prasad et al., 2005), and prairie-type soils (Mollisols) date from the Eocene (Retallack, 1982). Small, tubular root traces occur in paleosols corresponding to modern deserts and drylands (e.g., Aridisols and Vertisols) as early as the Devonian (Retallack, 1992). The general conclusion is that the late Paleozoic environments most likely to be dust sources had vegetative cover that was less effective at dust emission than comparable present-day environments, however, the quantitative details remain vague.

### The impact of model resolution, and some workarounds

Global climate modeling in deep time can require a large initial computational expense devoted to running the model for a sufficient time to enable the atmosphere to equilibrate with the ocean, a system with a long thermal memory. This computational expense motivates the use of lower-resolution grids when designing simulations that use a full, three-dimensional ocean (e.g., Heavens et al., 2015). At the same time, dust emission is highly non-linear in wind speed and so tends to be due to circulations from tens of meters to tens of kilometers in scale, much finer than the model resolution typical for deep-time studies (Cakmur et al., 2004).

There are two possible options to handling the under-resolution of dust emission. First, it may be ignored. Mahowald et al. (2006) found that choice of resolution introduced uncertainty comparable

to the choice between prescribing vegetation from an equilibrium vegetation model and using satellite data about vegetation. However, uncertainty in emission in both cases was less than 15% (Mahowald et al., 2006).

Second, it seems possible to correct under-resolved dust emission by predicting the statistical distribution of winds within a model grid cell (Newman et al., 2002; Ridley et al., 2013). Most dust emission comes from the rare, extreme winds in the distribution. Thus, if the dust emission parameterization integrates over the probability distribution of the wind, the dust emission still can be accurately predicted (Ridley et al., 2013). In principle, this approach is extendable to variations in surface properties such as vegetation cover.

Resolution, however, does not only affect emission. Cloud parameterizations are sensitive to horizontal resolution. Therefore, lower-resolution versions of the same model may use slightly different empirical factors in their cloud parameterizations so that their global radiative properties agree with observations (e.g., Yeager et al., 2006). One implication of this is that since the residence time of atmospheric dust is affected by cloud properties, the residence time can be an implicit function of resolution. This point is important to keep in mind when comparing the output of models that have different resolutions. It is also important to consider in radiatively active simulations, where a different residence time for large particles can affect longwave radiative forcing due to atmospheric dust.

### Fundamentals of dust cycle reconstruction

The classical approach to quantitative global dust cycle reconstruction remains that of Mahowald et al. (2006; also see Albani et al., 2015 for a more recent example). The approach has four steps. First, dust deposition data for a narrow time slice are compiled and quality assessed. The principle of compilation is that climate is relatively constant during the timeslice, as inferred from temperature and precipitation proxies. All of the data come from the geological record, thus age control is critical.

Second, the modeler identifies the key source regions for dust. These inferences have been made on the basis of the presence of significant loess, glacier fronts, glacial lake systems, or poorly vegetated ground (Mahowald et al., 2006). Another approach is to use geochemical or other data to infer the provenance/source region of the

dust (Delmonte et al., 2010; Soreghan et al., 2014).

Third, dust cycle simulations are run in which dust is a radiatively passive tracer in the atmosphere (so as not to disturb the model climate), and only one source region is allowed to emit dust at a time. Thus, the deposition of dust from each source is isolated. These simulations are known as source apportionment experiments. The dust cycle model is preferably validated by a control simulation that agrees with present-day observations of dust deposition and radiative forcing attributable to dust.

The fourth step is to tune the model to fit the data. If  $a_i$  is a linear factor called the source strength and corresponding to the  $i$ th source,  $M_{ij}$  are the dust deposition predictions for the  $i$ th source and the  $j$ th depositional site, and  $D_j$  is the dust depositional data for the  $j$ th site, then tuning seeks to minimize an appropriately weighted ( $w_j$ ) cost function of the basic form:

$$\sum_j w_j \left[ \left( \sum_i a_i M_{ij} \right) - D_j \right]^2 \quad \text{Eq. (1)}$$

Weighting of the cost function can take account of variations in data density so that the abundance of data in one area does not have outsized importance over areas where data are sparse. Weights also can be based on judgments about data quality. In one case, Mahowald et al. (2006) chose to consider ice cores as ten times more important than all other types of data sets. The weighting process is subjective and should be performed and interpreted with caution.

### Aeolian erodibility

The classical reconstruction described in the previous section yields quantitative estimates of the strength of dust sources. It sometimes requires the relative enhancement or diminution of some sources by orders of magnitude. It is not necessarily clear how this information should be interpreted. It is not as if the fundamental and well-characterized physics of dust emission should work more or less efficiently in different places. One interpretation conceptualizes this wide variability as something known as aeolian erodibility.

The correlation between climate variability and dust deposition is attributed to climatically driven changes in the efficiency with which the surface can be eroded by a given meteorological forcing (aeolian erodibility: Zender et al., 2003b; Kurosaki et al., 2011) as well as changes in the

intensity of the meteorological forcing (aeolian erosivity: Kurosaki et al., 2011), with aeolian erodibility appearing to be more important (Mahowald et al., 2006a). Put more simply, aeolian erodibility accounts for the principle that dust will not be emitted from a surface where dust-sized soil particles are not present and capable of being mobilized. In this simplified view of dust cycling, the effects of climate on transport or deposition are considered secondary. The classical reconstruction disentangles aeolian erosivity and erodibility, allowing erodibility to be interpreted.

It is therefore sometimes necessary to define a specific aeolian erodibility ( $S$ ) that incorporates systematic model biases as well as the difficult to model processes (salt crusting, soil grain-size evolution) that make some surfaces better dust emitters than others (Ginoux et al., 2001; Zender et al., 2003b; Mahowald et al., 2006), noting that parameterizations typically already include the inhibiting effects of soil moisture on dust mobilization. The specific aeolian erodibility then can be estimated from theoretical grounds or estimated from classical dust cycle reconstruction.

### Dust cycle reconstruction for the Late Paleozoic Ice Age

The classical approach was inappropriate for our LPIA dust cycle reconstruction for two reasons. First, the data were too sparse. At the scale of a global model, there are only five points with data, four of which are in western equatorial Pangea (Fig. 10A). Of these data points, two are continental and lack sufficient age control to determine the mass accumulation rate of dust. However, they are useful sources of provenance information. Second, the data points at which mass accumulation rates can be inferred are diachronous, which invalidates a strict definition of a timeslice (Fig. 10B). In addition, the only identified dust sources are two or three mountain ranges in central or western tropical Pangea (Soreghan et al., 2014). Our first step, therefore, was to determine what areas the model predicted to be source regions, and to understand the dependence of those source regions on climate. Using CCSM3 and the baseline climate simulations cited above, two sets of dust cycle experiments were modeled.

The model routines that simulate dust cycling are nearly identical to those described by Mahowald et al. (2006). The optical properties of dust are those used by Yoshioka et al. (2007).

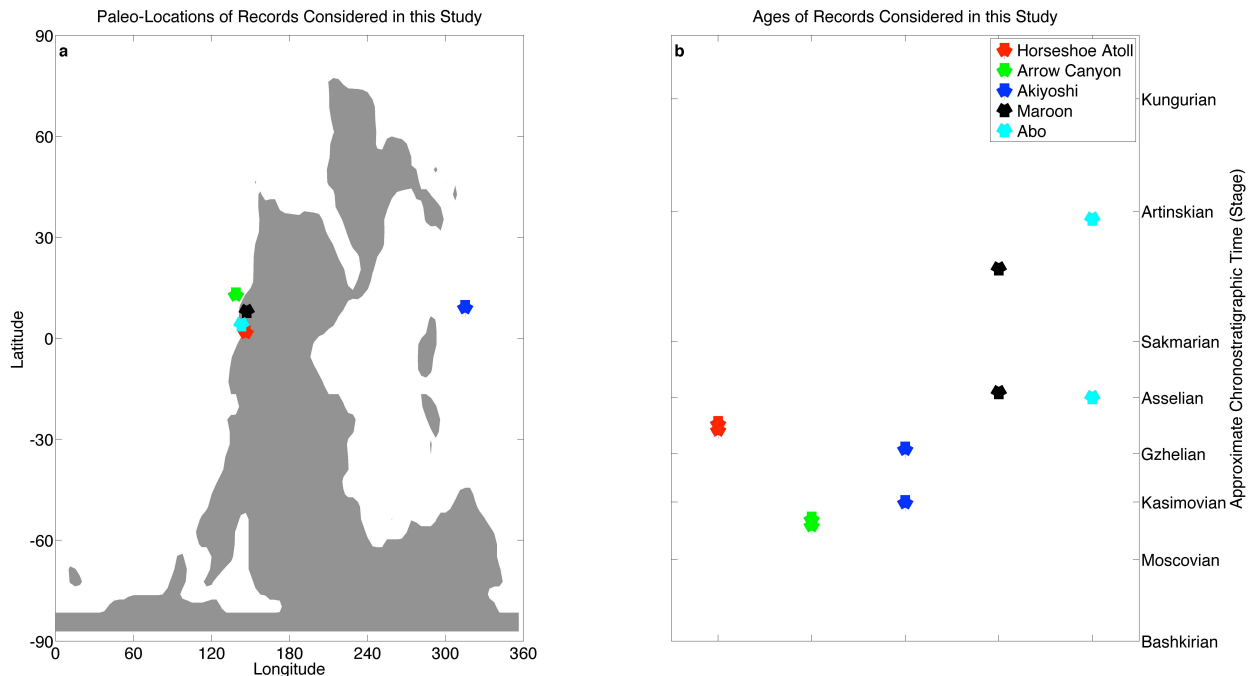


FIGURE 10.—Approximate locations of dust depositional records considered in this study in (A) paleogeographic space (Asselian–Sakmarian) and (B) chronostratigraphic time. Marine sites are indicated with downward-pointing triangles, while continental sites are marked with upward-pointing triangles.

Dust emission routines of Mahowald et al. (2006) were modified by increasing the vegetation area index (VAI) threshold for emission from  $0.1 \text{ m}^2 \text{ m}^{-2}$  to  $0.3 \text{ m}^2 \text{ m}^{-2}$ , following the analysis of Okin (2008) of the relationship between dust emission and lateral cover. Second, the size distribution of the emitted flux was modified. Mahowald et al. (2006) used a size distribution consistent with Grini and Zender (2004) and made the following assignment of the emitted flux to bins:  $0.1\text{--}1.0 \mu\text{m}$ , 3.8%;  $1.0\text{--}2.5 \mu\text{m}$ , 11%;  $2.5\text{--}5.0 \mu\text{m}$ , 17%; and  $5.0\text{--}10.0 \mu\text{m}$ , 67%. We modified the size distribution to agree with the observationally validated physical model of Kok (2011):  $0.1\text{--}1.0 \mu\text{m}$ , 1.1%;  $1.0\text{--}2.5 \mu\text{m}$ , 8.7%;  $2.5\text{--}5.0 \mu\text{m}$ , 27.7%; and  $5.0\text{--}10.0 \mu\text{m}$ , 62.5%. Note that this latter distribution shifts the distribution to larger sizes, which enhances longwave radiative forcing for the same mass of dust.

Dust was treated as radiatively passive, and  $S$  was set to a uniform value of  $0.0651 (\text{kg m}^{-2} \text{s}^{-1}) (\text{kg m}^2 \text{s}^{-1})^{-1}$  over all land areas and to zero over the ocean. The uniform value of  $S$  chosen is equivalent to the global land average  $S$  according to the geomorphic erodibility hypothesis of Zender et al. (2003b), so that global dust emission, mean dust optical depth at 670 nm (AOD), and other model output would take reasonable values.

In the first set of experiments (unadjusted), model routines that simulate dust used the vegetation information associated with the baseline climate simulations of Heavens et al. (2015). However, these simulations only use two vegetation maps generated by the equilibrium vegetation model BIOME4. One map corresponds to  $\text{CO}_2$  levels of 2500 ppmv. The other map corresponds to  $\text{CO}_2$  levels of 250 ppmv, but without permanent land ice. Therefore, these maps limit vegetation scenarios to global climates that are relatively warm compared to the dusty climates of Neogene glacials.

In the second set of experiments (adjusted vegetation), model routines that simulate dust used vegetation information associated with BIOME4 simulations forced by the baseline climate simulations themselves. The vegetation information that affects CCSM3 as a whole (albedo, transpiration, roughness, etc.) was left unchanged. The only change was the input to the vegetation thresholds mentioned above.

These experiments show that the principal sources of dust were the subtropical deserts of Pangea (Figs. 11, 12). Source areas were larger under colder climate. The slight reduction in source area in the coldest simulation (Figs. 11D, 12D) was due to the encroachment of an ice sheet into the subtropical deserts. The predicted sources

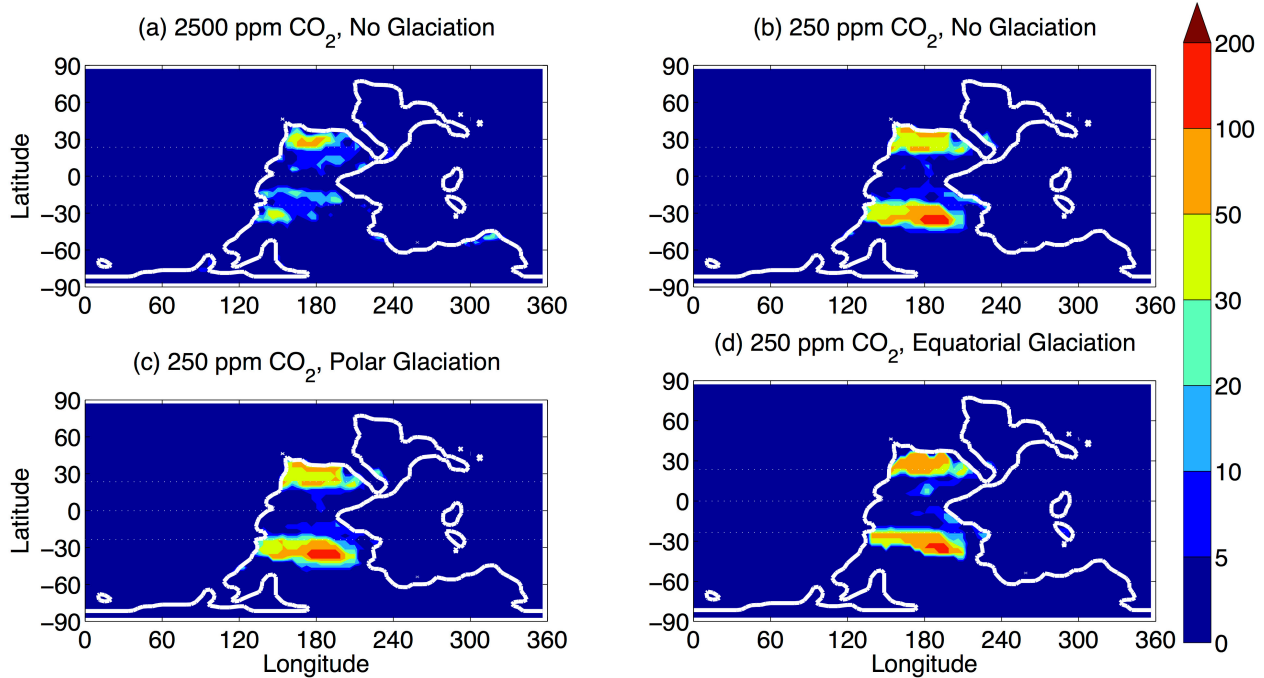


FIGURE 11.—Annual dust emission ( $\text{g m}^{-2} \text{ yr}^{-1}$ ) for the unmodified uniform erodibility dust cycle experiments for four baseline climate simulations, as named in Heavens et al. (2015): A) greenhouse.noglaciation; B) icehouse.noglaciation; C) icehouse.glaciation.polar; D) icehouse.glaciation.equatorial. Horizontal white lines mark the Equator and each tropic.

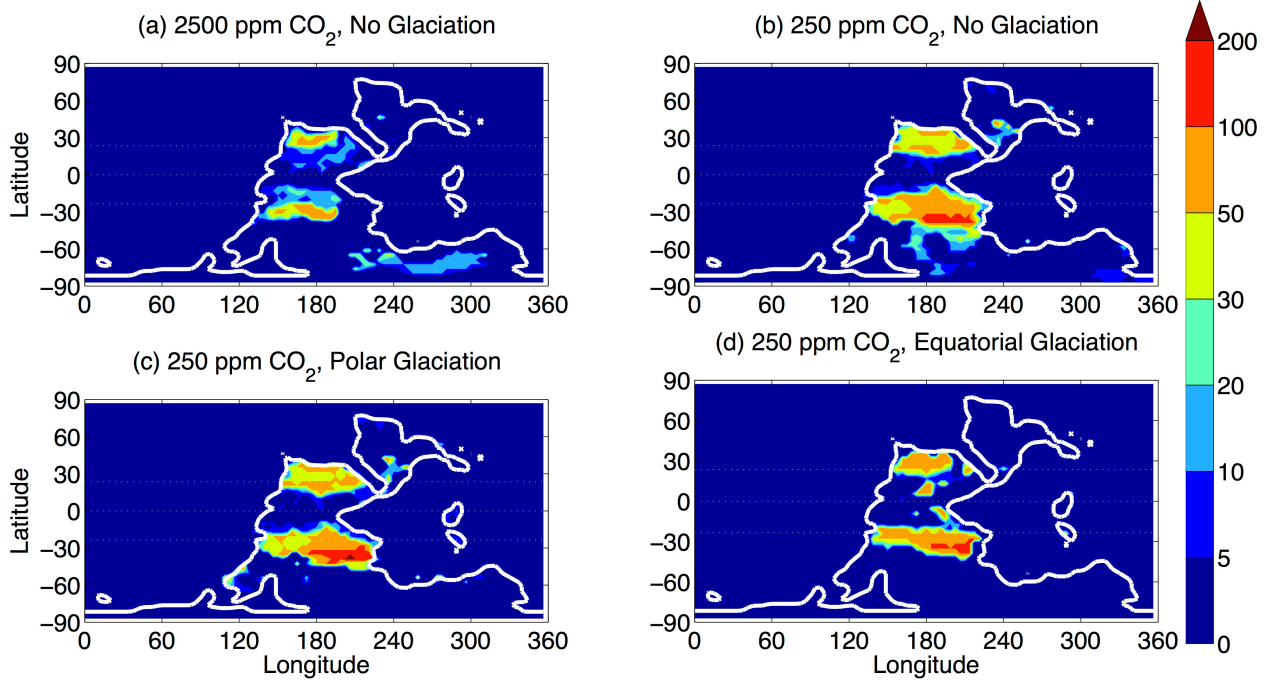


FIGURE 12.—Annual dust emission ( $\text{g m}^{-2} \text{ yr}^{-1}$ ) for the adjusted vegetation uniform erodibility dust cycle experiments for four baseline climate simulations, as named in Heavens et al. (2015): A) greenhouse.noglaciation; B) icehouse.noglaciation; C) icehouse.glaciation.polar; D) icehouse.glaciation.equatorial. Horizontal white lines mark the Equator and each tropic.

for the high CO<sub>2</sub> simulations (Figs. 11A, 12A), however, violate a standard hypothesis about greenhouse climate during the Permian. In these simulations, the dust source regions in the northern and southern tropics are distinct, and little dust is sourced from the Equator. This contradicts the idea that tropical Pangea was a single, latitudinally continuous arid region due to megamonsoonal atmospheric circulation (Kutzbach and Gallimore, 1989; Boucot et al., 2013). This possible error is characteristic of CCSM3 applied to Permian conditions. Kiehl and Shields (2005) simulated a similarly wet equator under high CO<sub>2</sub> conditions (~ 3500 ppmv). Note that the GENESIS model has reproduced a large equatorial arid region under high CO<sub>2</sub> conditions (Peyser and Poulsen, 2008).

Also, in the coldest simulation (Figs. 11D, 12D), a significant dust source appears near 10° N, 180° E. This source is especially enhanced in the adjusted vegetation simulations, reflecting the importance of vegetation change from forest to savannah (or appropriate Paleozoic analog) in activating this dust source. This area roughly corresponds to part of the Central Pangean Mountains, a possible area of importance for weathering of Grenvillean-aged material exposed by the Alleghanian orogen. This material is generally thought to be a key source of atmospheric dust to the Ancestral Rocky Mountains during glacials (Soreghan et al., 2014).

#### The path to reconstruction: dynamic soil erodibility and the pulsed glacial source

Owing to limited data, one approach to reconstruction might be to reduce the number of degrees of freedom of the problem by specifying the relative soil erodibility and then tuning to the data to obtain the absolute soil erodibility ( $S$ ). Theoretical approaches to estimating  $S$  (Zender et

TABLE 3.—Composite glacial and interglacial mass accumulation rates (MAR) for 0.1–10 μm fraction.

	Latitude in Model Grid (°)	Longitude in Model Grid (°)	Minimum Interglacial MAR (gm <sup>-2</sup> yr <sup>-1</sup> )	Maximum Interglacial MAR (gm <sup>-2</sup> yr <sup>-1</sup> )	Minimum Glacial MAR (gm <sup>-2</sup> yr <sup>-1</sup> )	Maximum Glacial MAR (gm <sup>-2</sup> yr <sup>-1</sup> )	Minimum Glacial/ Interglacial Ratio <sup>1</sup>
Horseshoe Atoll	2	146	0.013	0.037	12.7	127	340
Arrow Canyon	13	139	0.02	0.26	7.55	15.1	30
Akiyoshi Atoll	9	315	0.0013	0.0026	0.038	0.075	15

<sup>1</sup>Minimum glacial/interglacial ratio is the ratio between Minimum Glacial MAR and Maximum Interglacial MAR.

al., 2003b), however, probably require more detailed information about topography and precipitation than are available for the LPIA.

The approach taken here was to speculate that episodes of high dust deposition during the time interval corresponding to maximum glaciation or the first stages of deglaciation indicate the rapid loss of dust from special source areas where it accumulated during most of a glacial–interglacial cycle. Dust deposition at other times reflects emission from background source areas, where dust availability is more limited. In this case, we assumed that the area around 10° N, 180° W (the foothills of the Central Pangean Mountains) is a good example of a special source area. What follows is that the icehouse.glaciation.equatorial simulation of Heavens et al. (2015) corresponds to the end of glacials, while its closest, warmer baseline climate simulation (icehouse.glaciation.polar) corresponds to the interglacials. A smaller range in climate certainly would have been preferable, but we needed to rely upon the baseline climate simulations we had performed.

Data are available at each marine site about the variability of dust deposition over the course of a glacial–interglacial cycle. The data were therefore organized so that a range of dust deposition rates for interglacial conditions and for the dusty conditions observed at the glacial termini could be estimated (Table 3).

The glacial–interglacial variability in most of the extant depositional records was matched using the following procedure to generate a pulsed glacial source reconstruction. Dust cycling simulations were run with uniform aeolian erodibility fully climate-adapted vegetation, and radiatively passive dust for the interglacial and glacial baseline climate simulations (hereafter X<sub>I</sub> and X<sub>G</sub>). The vegetation in these simulations is

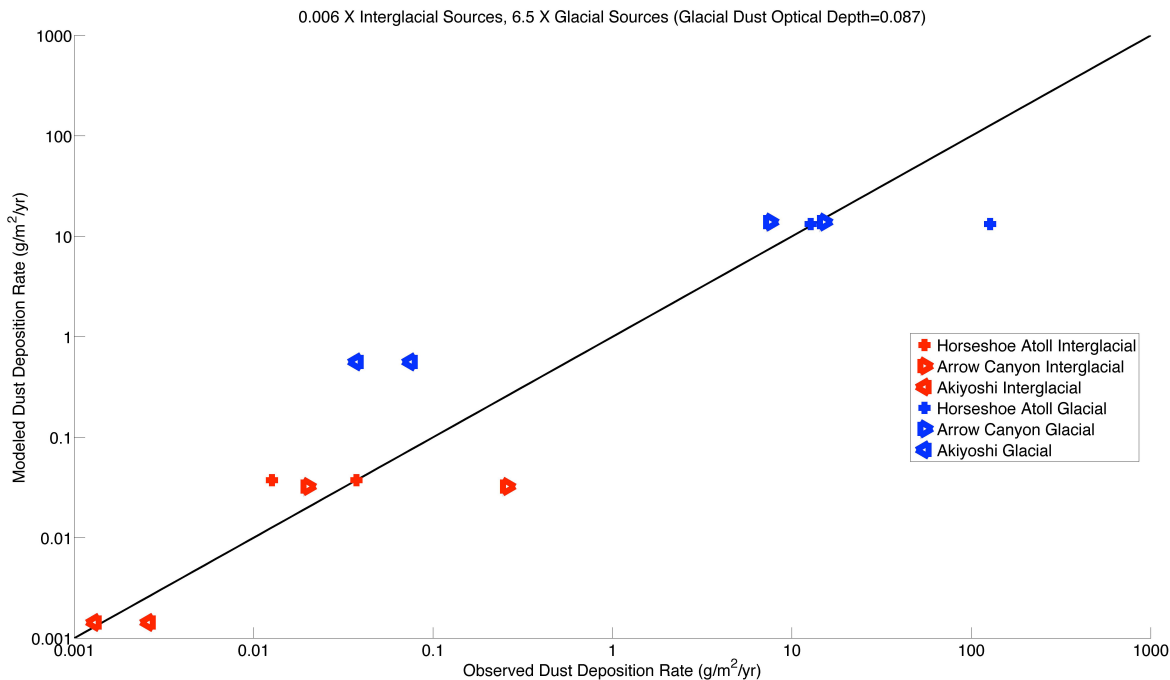


FIGURE 13.—Scatterplot comparing observed and modeled dust deposition rates in the pulsed glacial source reconstruction of aeolian erodibility. The global mean dust optical depth at 660 nm is at the top.

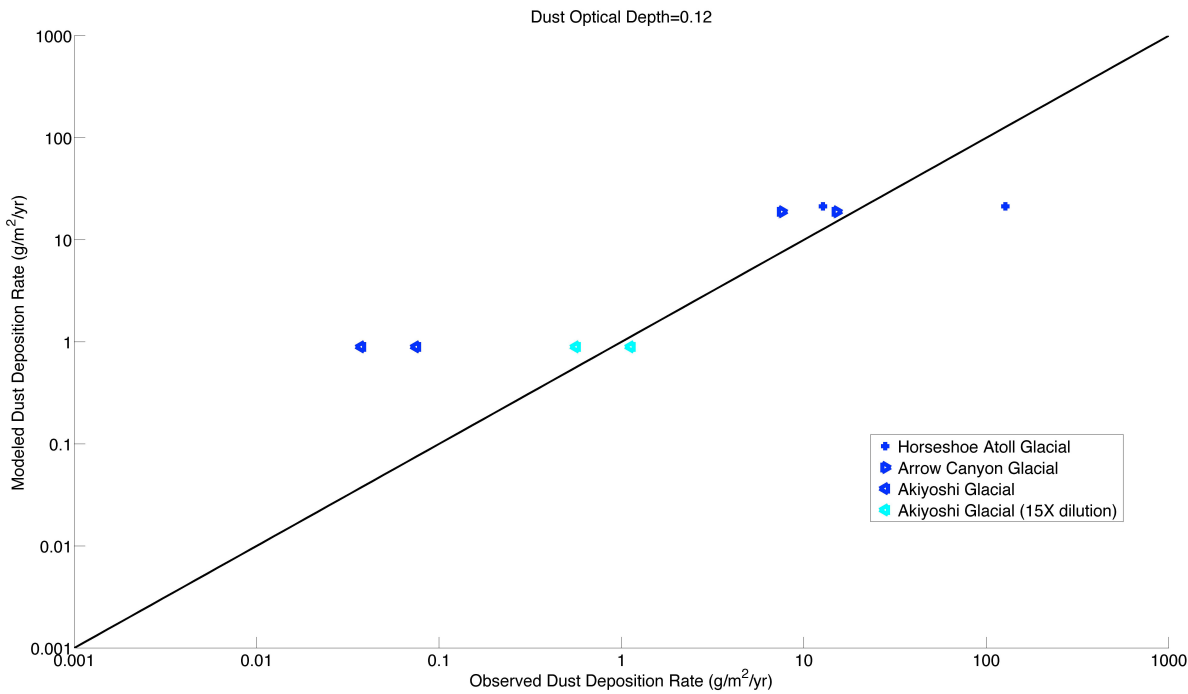


FIGURE 14.—Scatterplot comparing observed and modeled dust deposition rates for the pulsed glacial source reconstruction with radiatively active dust. The global mean dust optical depth at 660 nm is at the top.

the same as in the climate adjusted vegetation simulations, but is allowed to modify albedo, evapotranspiration, and surface roughness directly. This change has a minimal effect on the global properties of the model climate and the

amplitude and spatial distribution of dust sources. These simulations then were compared to determine which dust sources emitted more strongly during interglacials than glacials (“the interglacial sources”) and which dust sources

emitted more strongly during glacials than interglacials ("the glacial sources"). Dust deposition due to glacial sources alone was then determined by running a dust cycle simulation under the glacial baseline climate in which  $S$  for all but the glacial sources was set to zero ( $Y_G$ ). The dust deposition rates predicted by these three simulations were then weighted (by inspection) to match the depositional data (Fig. 13). That is, glacial deposition ( $D_G$ ) was modeled as:

$$D_G = f_g(M_{Y_G}) + f_i(M_{X_G} - M_{Y_G}) \quad \text{Eq. (2)}$$

while interglacial deposition was modeled as:

$$D_I = f_I(M_{Y_I}) \quad \text{Eq. (3)}$$

where  $f_G$  and  $f_I$  are the weights/ tuning factors.

This procedure effectively tunes down the interglacial sources under both glacial and interglacial conditions but tunes up the glacial sources only under glacial conditions. The principal misfit is over-prediction of glacial deposition in the Akiyoshi (Japan; Fig. 13), where glacial deposition could be underestimated because of smearing of the dust pulse signal in an environment of low carbonate accumulation but significant bioturbation and wave mixing (see above). It is, therefore, a compromise between two impractical approaches. The erodibility of all sources in each baseline climate simulation could have been tuned to match the marine depositional records, but this would have lacked any physical justification and downplayed the change to the Central Pangean Mountain source. The alternative at the other extreme would have been to define glacial sources as sources that emit only during glacials while using a consistent value of specific aeolian erodibility ( $S$ ) for glacial sources between climate scenarios. This approach would have ignored most of the intensification of the Central Pangean Mountain source.

The next step is to determine if the reconstruction holds when the response of climate to dust is considered. To do this, soil erodibility was adjusted to the values obtained by tuning, and the dust cycle simulation was run for the glacial baseline climate. In this case, global climate becomes significantly dustier. Estimated dust deposition is just higher than the envelope for the Arrow Canyon (Nevada) data point, and on the low end of the envelope for the Horseshoe Atoll

(Texas) data point. The rate of glacial dust deposition for the Akiyoshi does not agree with the reconstruction. However, if we assume that depositional factors have diluted the glacial peak in dust deposition by a factor of 15, agreement with the reconstruction is obtained (Fig. 14). If the reconstruction had changed too dramatically, the glacial source tuning factor would have been reduced and tried again. Note that the strong feedback reflects high longwave radiative forcing. This radiative forcing is somewhat unrealistic, and attributable to using the low resolution CCSM3 (T31x3) (see Yeager et al., 2006) and a size distribution for emitted dust with slightly larger particles than in Mahowald et al. (2006). One possible approach to this problem is to adjust the dust optical properties so that the longwave radiative forcing per unit optical depth (radiative forcing efficiency) for a modern simulation matches present-day observations. Because of this issue, we omit any discussion of the radiative forcing implied by the reconstruction.

The reconstruction makes predictions about the significant dust source regions, including subtropical deserts in Pangea, a single area in the northern hemisphere, and sources in both western and eastern Pangea in the southern hemisphere (Fig. 15). There also are significant tropical sources, including at 10° N, 180° E, along the axis of the Central Pangean Mountains as far as the Hercynian orogen, and in northeastern South America and northwestern Africa. Minor sources occur in the Ancestral Rocky Mountains and nearby volcanic terranes, consistent with provenance information (Soreghan et al., 2014).

Annual deposition and optical depth maps suggest a dusty world (Fig. 16). Dust optical depth is predicted to be five or six times that of the present day (Fig. 16A). Significant dust plumes are inferred for the Panthalassic Ocean off of the west coast of Pangea, in Paleo-Tethys off of the east coast of southern subtropical Pangea, and in the Uralian seaway (Fig. 16B). Areas of high deposition over the ocean are particularly notable in wet deposition, emphasizing that much dust deposited over the ocean is likely subject to some sort of processing within clouds (Fig. 16D).

The extent of dustiness in the reconstruction is best illustrated by examining mean dust optical depth in a single month: December. Here, a continuous area of optical depth  $> 0.5$  is observed across all of southern tropical Pangea and the adjoining waters (Fig. 17). Within this region, there are areas with optical depth  $> 1$ . There is

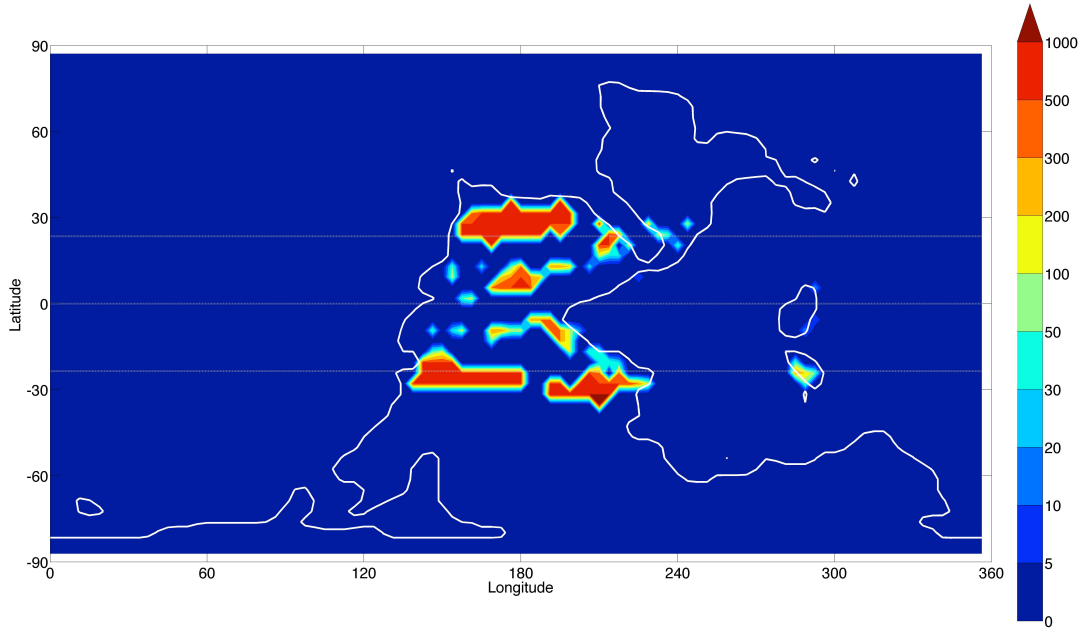


FIGURE 15.—Annual dust emission ( $\text{g m}^{-2} \text{yr}^{-1}$ ) for the pulsed glacial source reconstruction with radiatively active dust. Horizontal white lines mark the Equator and each tropic.

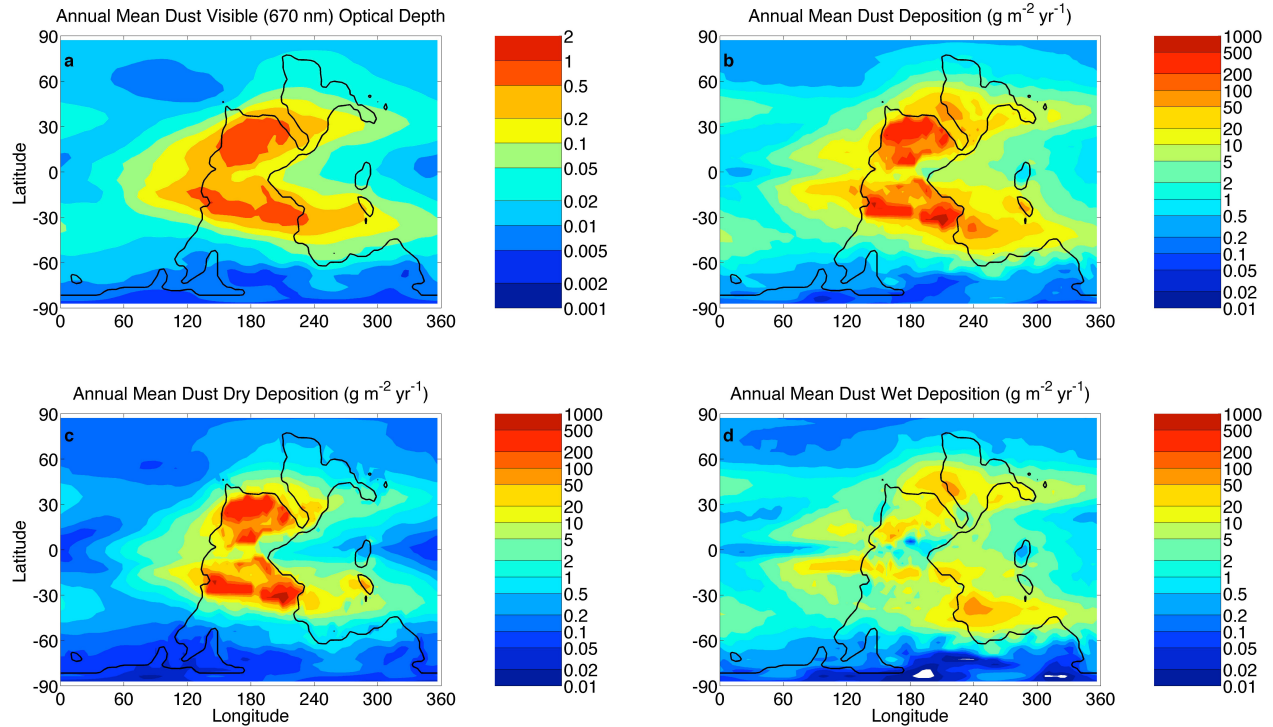


FIGURE 16.—Annual mean characteristics for the pulsed glacial source reconstruction with radiatively active dust.

also an equatorial region with similar optical depth. During the “super dust storm” event of March 2012, the dustiest land observation sites in the Arabian Peninsula had mean dust aerosol optical depths of  $\sim 0.75$  (Alam et al., 2014). Given

that this event resulted in hundreds of hospitalizations for respiratory distress (Alam et al., 2014), it seems possible that some vertebrate populations in Pangea experienced respiratory distress on a frequent basis.

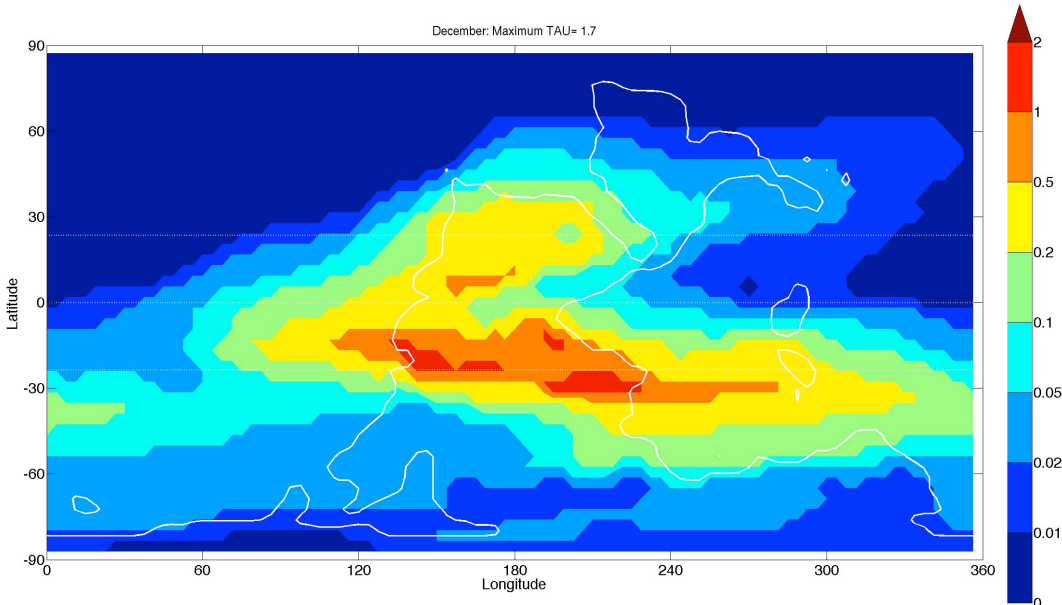


FIGURE 17.—Mean visible (660 nm) dust optical depth for December for the pulsed glacial source reconstruction with radiatively active dust. The maximum value in a grid cell is in the title.

## THE IMPACT OF DUST ON THE BIOSPHERE

### Biogeochemical modeling of marine dust fertilization

Dust transport can have biogeochemical impacts on land, e.g., renewal of nutrients in island soils (Chadwick et al., 1999; Okin et al., 2004). However, much of the focus on the impact on dust on biogeochemistry has focused on the marine realm, where atmospheric dust could have a variety of impacts. Dust can directly stimulate biological productivity by providing Fe and other trace nutrients to organisms with an enzymatic requirement for them (Martin et al., 1991; Okin et al., 2011). Productivity by these organisms can increase the nutrient supply in other ways (e.g., fixing N), stimulating productivity of other organisms.

The role of dust is not always positive. Dust may transport pathogens long distances to areas where organisms lack antibodies (Shinn et al., 2000). In addition, dust and the organisms whose productivity it stimulates clouds water, reducing the light available to coral zooxanthellae and deep-dwelling photosynthesizers in general (Hallock and Schlager, 1986; Shinn et al., 2000).

As a first step to quantifying the potential impact of LPIA dust on biogeochemistry, we used the pulsed glacial source reconstruction with radiatively active dust as input for a simple biogeochemical model of dust fertilization,

mostly following the approach of Okin et al. (2011) for estimating the biogeochemical impact of dust in the present-day climate. It is assumed that carbon fixation is controlled by phosphorus limitation, and diazotrophs will manufacture needed nitrogen given sufficient iron in environments similar to modern high-nitrate low-chlorophyll (HNLC) waters. This applies the idea that high dust delivery makes the ocean P-limited (Moore and Doney, 2007).

Following Okin et al. (2011), carbon fixation due to dust fertilization was initially estimated as proportional to the deposition rate of bioavailable Fe in ice-free HNLC waters ( $[NO_3^-] > 4 \mu M$ ). Dust is assumed to be 3.5% Fe by mass (Luo et al., 2008), and 21.5% bioavailable (soluble) for wet deposition and 1% for dry deposition. The estimated bioavailability for wet deposition is the average Fe solubility of dust in rain and snow samples surveyed by Moxim et al. (2011), while that for dry deposition is the low end measured in aerosol samples reported by Moxim et al. (2011). Note that techniques exist for modeling bioavailability within the dust transport parameterization (Moxim et al., 2011). Also note that Baker and Jickells (2006) downplayed the role of cloud processing in bioavailability/solubility and instead argued that solubility is a strong inverse function of size. At present, both of these are valid approaches to estimating solubility.

We adapted the paleogeographic approach to aerosol prescription of Heavens et al. (2012) in

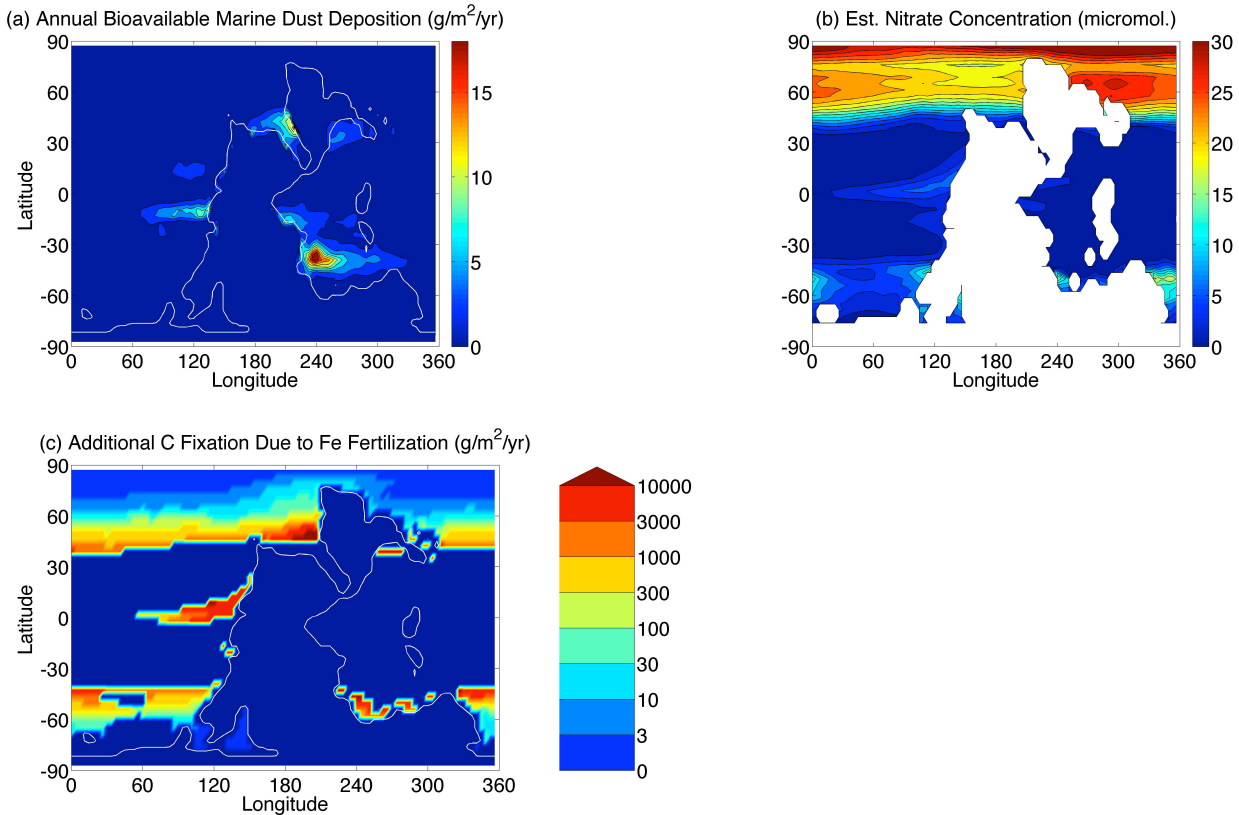


FIGURE 18.—Biogeochemical implications of the pulsed glacial dust cycle reconstruction with radiatively active dust A) Estimated annual deposition of dust with soluble Fe ( $\text{g m}^{-2} \text{ yr}^{-1}$ ); B) Paleogeographic prescription of surface water  $[\text{NO}_3^-]$  for the LPIA; C) Additional carbon fixation due to iron fertilization ( $\text{g m}^{-2} \text{ yr}^{-1}$ ).

order to estimate nutrient concentrations in the ocean. Late Paleozoic nitrate concentrations were estimated from LEVITUS94 dataset values at 10 m in the modern ocean (Conkright et al., 1994). Nitrate concentrations in the Late Paleozoic were estimated from the zonal mean and standard deviation of sea surface temperature in the climate simulation, which then was scaled with the zonal mean and standard deviation of nitrate concentration in the LEVITUS94 dataset. (Anomalously cool waters contain anomalous concentrations of nitrate and vice versa.) Because the bulk of the continental area today is in the Northern Hemisphere but was in the Southern Hemisphere in the early Permian, the modern dataset was first flipped upside down (note that flipping does not significantly impact the global estimate of carbon fixation). Phosphate was then estimated by assuming N:P in water is at the Redfield ratio of 16:1.

Carbon fixation rates estimated by this method are up to  $30000 \text{ g m}^2 \text{ yr}^{-1}$ , implying P-limitation is likely. This calculation was then corrected for photic zone P-limitation by limiting

C-fixation by the rate that can be supported by phosphate availability in a 100 m photic zone, assuming C:P in fixed organic matter is at the Redfield ratio of 106:1. Paytan and McLaughlin (2007) estimated P remineralization occurs in < 1 day to two weeks; we assumed 10 days. This correction reduces the maximum rates of carbon fixation to <  $11000 \text{ g m}^2 \text{ yr}^{-1}$ . Assuming monthly dust deposition only over ice-free surfaces, the result is 72 Pg/yr of C fixation (or roughly 140% of the present day value of C fixation in the ocean). This calculation implies that if the ocean during the LPIA had similar basic nutrient levels as today and our reconstruction of marine deposition is sufficiently accurate, LPIA glacial intervals would have been periods of extreme marine productivity (Fig. 18).

#### Reefs during the dust-rich late Paleozoic

Reefs are volatile biotic structures. Many times over the Phanerozoic, reefs have expanded quickly and suddenly collapsed, presumably in response to a mixture of biotic and environmental change (Kiessling, 2009). Accompanying the

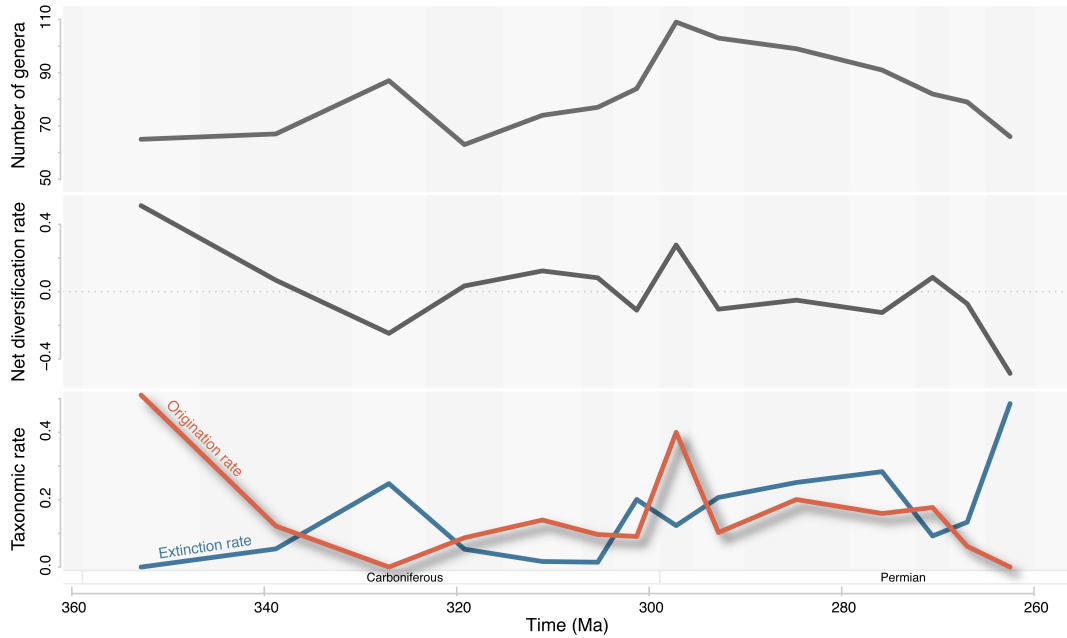


FIGURE 19.—Patterns of diversity dynamics of late Paleozoic corals. The number of genera is shown in the top panel and is calculated based on the number of genera that range into an interval. The net diversification rate (middle panel) is equal to the origination rate minus extinction rates (broken out in the bottom panel). Gray bars in the background indicate geological epochs. C = Carboniferous; P = Permian.

volatility in the frequency and volume of reefs is transformation of the taxonomic composition of reefs. Microbes, algae, and hypercalcifying animals, such as sponges, bryozoans, and corals, can build reefs. Reefs dominated by each group wax and wane, but corals and sponges tend to dominate in times of the major building of expansive reefs during the Silurian, Devonian, Triassic, Jurassic, and Neogene.

Reefs during the late Paleozoic and Cretaceous both fall between two of these major reef-building pulses. Along with the Cretaceous nadir in reef building, reefs in the late Paleozoic are not particularly extensive or numerous. Reefs in the Cretaceous were dominated by rudist bivalves. Even though contemporaneous scleractinian corals were diverse and common; they simply did not build many reefs. In contrast, late Paleozoic reefs were dominated by algae and bryozoans, and shifted away from coral- and sponge-dominated reefs (Kiessling, 2009).

Throughout the Phanerozoic, reefs usually formed in nutrient-poor settings (Kiessling, 2009). Late Paleozoic reefs are strikingly different in this regard throughout the Carboniferous and into the early Permian, when phylloid algae dominated reefs. During the late Carboniferous and early Permian, these algal reefs maintained a wide latitudinal extent, ranging north up to 50 degrees

paleolatitude (Kiessling, 2001). Algal reefs are expected to occur in eutrophic settings, but these reefs do not occur near expected zones of upwelling (Kiessling et al., 1999). Rather, algal reefs temporally coincide with increased dustiness and common occurrence of dust deposits (Soreghan and Soreghan, 2002).

The algal reefs that fringed the northern margin of Laurentia during the late Paleozoic (Watkins and Wilson, 1989; Kiessling et al., 1999; Soreghan and Soreghan, 2002) occurred near the major zones of expected dust sources (Fig. 17). The most likely hypothesis for algal domination of reefs during this time is the high nutrient influx from these dusty conditions that would have promoted algal over coral reef building.

Precisely how this transition from coral to algal reef building played out remains uncertain. Two overlapping hypotheses are possible, depending on how corals respond to nutrient increases. In the extreme case, nutrient increases could produce the extinction of corals globally. Alternatively, local extirpation of corals could occur as corals shifted ranges to areas less affected by dusty, high-nutrient conditions. In this second extirpation case, corals may survive and relocate, but may or may not retain their reef-building activities.

As a first-order test to distinguish between the

global extinction and local extirpation hypothesis evidence of elevated global extinction rates can be examined through the Late Paleozoic. Genus-level occurrence data were downloaded from the Paleobiology Database (<http://paleobiodb.org>) to explore this issue. Figure 19 shows rugose and tabulate coral diversity dynamics through the Carboniferous and Permian (excluding the end Permian mass extinction). During the Serpukhovian, there is a slight extinction pulse and a decline in origination rates of coral genera, which results in a negative net diversification rate (origination minus extinction). This results in a diversity decline in the lower Pennsylvanian. After a brief positive diversification pulse in the earliest Permian caused by a burst of origination, there is a slight but consistent pattern of negative net diversification rates that persists for three stages.

The diversification dynamics shown in Fig. 19 suggest that the pattern of global extinction is inconsistent over the intervals of dustiness. At times, diversification rates remain positive, but at other times, rates are slightly negative. In both cases, a large number of coral genera remain through the interval. As a consequence, the more local pattern of coral range shifts, and local extirpation needs to be mapped explicitly in order to understand how corals lost reef-building dominance during the late Paleozoic.

Dust is thought to play a negative role in the health of coral reefs today (e.g., Garrison et al., 2003). Historically however, other important causes of reef collapse are apparent. The collapse of Caribbean reefs have largely been due to the consequences of over fishing (Jackson et al., 2014). What is relevant here is the part that algae play in this reef collapse. The loss of grazing fish leads to an explosion of macro algae on reefs, resulting in a loss of coral recruitment and an increase in coral disease (Jackson et al., 2014). This suggests that during the late Paleozoic, coral loss may have more to do with the rise of algae than as a direct inhibition of coral growth by dust. If a rise in algae acted to cause coral extirpation, a protracted negative interaction between corals and algae that plays out over space and time would be expected.

## CONCLUSIONS

Dust is a key element in today's Earth system, and should have been in deep time as well, perhaps especially during icehouse intervals of Earth

history. It forms both an archive and agent of climate and climate change, recording sub-Milankovitch (millennial) resolution of atmospheric dustiness and circulation. Climate models of atmospheric dustiness expand predictions of source regions from even limited deep-time data points, and help address the significant impact of dust on both the physical climate system and biosphere. Finally, dust holds strong potential to impact primary productivity and thus carbon cycling in both marine and continental systems. The late Paleozoic Earth System appears to have been a particularly dusty interval of Earth history, and preliminary data suggest we have much to learn about Earth and life from mining dust records in deep time.

## ACKNOWLEDGMENTS

We thank the organizers of this GSA Short Course, especially D. Polly, for the direction and motivation to prepare this contribution as part of the NSF's "Earth-Life-Transitions" program. Funding for this research was provided by the National Science Foundation (EAR-1053018, EAR-1338331 to GSS, EAR-1337463 to NGH, EAR-1543518 to LAH, and EAR-1337440 to SMA). We thank D. Polly and J. Mason for constructive reviews that improved the manuscript.

## REFERENCES

- Aarons, S. M., S. M. Aciego, and J. Gleason. 2013. Variable Hf-Sr-Nd radiogenic isotopic compositions in a Saharan dust storm over the Atlantic: Implications for dust flux to oceans, ice sheets and the terrestrial biosphere. *Chemical Geology*, 349–350:18–26.
- Abrajevitch, A., A. P. Roberts, and K. Kodama. 2014. Volcanic iron fertilization of primary productivity at Kerguelen Plateau, Southern Ocean, through the Middle Miocene Climate Transition. *Paleogeography, Paleoclimatology, Paleoecology*, 410:1–13.
- Aciego, S. M., B. Bourdon, M. Lupker, and J. Rickli. 2009. A new procedure for separating and measuring radiogenic isotopes (U, Th, Pa, Ra, Sr, Nd, Hf) in ice cores. *Chemical Geology*, 266:203–213.
- Aciego, S. M., E. I. Stevenson, and C. A. Arendt. 2015. Climate versus geological controls on glacial meltwater micronutrient production in southern Greenland. *Earth and Planetary Science Letters*, 424:51–58.

- Alam, K., T. Trautmann, T. Blaschke, and F. Subhan. 2014. Changes in aerosol optical properties due to dust storms in the Middle East and Southwest Asia. *Remote Sensing of Environment*, 143:216–227.
- Albani, S., N. M. Mahowald, G. Winckler, R. F. Anderson, L. I. Bradtmiller, B. Delmonte, R. François, M. Gorman, N. G. Heavens, P. P. Hesse, S. A. Hovan, S. Kang, K. E. Kohfeld, H. Lu, V. Maggi, J. A. Mason, P. A. Mayewski, D. McGee, X. Miao, B. L. Otto-Btiesner, A. T. Perry, A. Pourmand, H. M. Roberts, N. Rosenbloom, T. Stevens, and J. Sun. 2015. In press. Twelve thousand years of dust: the Holocene global dust cycle constrained by natural archives. *Climate of the Past*.
- An, Z. (ed). 2014. Late Cenozoic Climate Change in Asia: Loess, Monsoon and Monsoon-Arid Environment Evolution, Springer-Verlag, Dordrecht.
- An, Z. S., J. E. Kutzbach, W. L. Prell, and S. C. Porter. 2001. Evolution of Asian monsoons and phased uplift of the Himalaya-Tibetan plateau since late Miocene times. *Nature*, 411:62–66.
- Anklin, M., J. Schwander, B. Stauffer, J. Tschumi, A. Fuchs, J. M. Barnola, and D. Raynaud. 1997. CO<sub>2</sub> record between 40 and 8 kyr B.P. from the Greenland Ice Core Project ice core. *Journal of Geophysical Research*, 102:26539–26545.
- Antoine, P., D.-D. Rousseau, O. Moine, S. Kunesch, C. Hatte, A. Lang, H. Tissoux, and L. Zoller. 2009. Rapid and cyclic aeolian deposition during the Last Glacial in European loess: a high-resolution record from Nussloch, Germany. *Quaternary Science Reviews*, 28:2955–2973.
- Arendt, C. A., S. M. Aciego, and E. A. Hetland. 2015. An open source Bayesian Monte Carlo isotope mixing model with applications in Earth surface processes. *Geochemistry Geophysics Geosystems*, 16:1274–1292.
- Arendt, C. A., S. M. Aciego, K. W. W. Sims, and M. Robbins. 2014. Sequential separation of uranium, hafnium and neodymium from natural waters concentrated by iron coprecipitation. *Geostandards and Geoanalytical Research*, 39:293–303.
- Arnalds, O. 2010. Dust sources and deposition of aeolian materials in Iceland. *Icelandic Agricultural Sciences*, 23:3–21.
- Assallay, A. M., C. D. F. Rogers, I. J. Smalley, and I. F. Jefferson. 1998. Silt: 2–62 µm, 9–4 φ. *Earth Science Reviews*, 45:61–88.
- Bagnold, R. A. 1941. The Physics of Blown Sand and Desert Dunes. Chapman and Hall, London.
- Baker, A. R., and T. D. Jickells. 2006. Mineral particle size as a control on aerosol iron solubility. *Geophysical Research Letters*, 33:L17608.
- Bayon, G., K. W. Burton, G. Soulet, N. Vigier, B. Dennielou, J. Etoubleau, E. Ponzevere, C. R. German, and R. W. Nesbitt. 2009. Hf and Nd isotopes in marine sediments: Constraints on global silicate weathering. *Earth and Planetary Science Letters*, 277:318–326.
- Berger, A., and M.-F. Loutre. 1994. Astronomical forcing through geologic time, p. 15–24. *In* P. L. de Boer and D. G. Smith (eds), Orbital Forcing and Cyclic Sequences, International Association of Sedimentologists, Special Publication, 19.
- Berger, A., M.-F. Loutre, and J. Laskar. 1992. Stability of the astronomical frequencies over Earth's history for paleoclimate studies. *Science*, 255:560–566.
- Berner, R. A., and Z. Kothavala. 2001. GEOCARB III: A revised model of atmospheric CO<sub>2</sub> over Phanerozoic time. *American Journal of Science*, 301:182–204.
- Bigelow, N. H., L. B. Brubaker, M. E. Edwards, S. P. Harrison, I. C. Prentice, P. M. Anderson, A. A. Andreev, P. J. Bartlein, T. R. Christensen, W. Cramer, J. O. Kaplan, A. V. Lozhkin, N. V. Matveyeva, D. F. Murray, A. D. McGuire, V. Y. Razzhivin, J. C. Ritchie, B. Smith, D. A. Walker, K. Gajewski, V. Wolf, B. H. Holmqvist, Y. Igarashi, K. Kremenetskii, A. Paus, M. F. J. Pisaric, and V. S. Volkova. 2003. Climate change and Arctic ecosystems: 1. Vegetation changes north of 55° N between the last glacial maximum, mid-Holocene, and present. *Journal of Geophysical Research*, 108:8170.
- Bills, B. G. 1994. Obliquity-oblateness feedback: are climatically sensitive values of obliquity dynamically unstable? *Geophysical Research Letters*, 21:177–180.
- Blichert-Toft, J., N. T. Arndt, and G. Gruau. 2004. Hf isotopic measurements on Barberton komatiites: effects of incomplete sample dissolution and importance for primary and secondary magmatic signatures. *Chemical Geology*, 207, 261–275.
- Boucot, A. J., C. Xu, and C. R. Scotese. 2013. Phanerozoic Paleoclimate: An Atlas of Lithologic Indicators of Climate. SEPM Concepts in Sedimentology and Paleontology, 11.
- Boyce, C. K., T. J. Brodribb, T. S. Field, and M.A. Zwieniecki. 2009. Angiosperm leaf vein evolution was physiologically and environmentally transformative. *Proceedings of the Royal Society B*, 276:1771–1776.
- Boyd, P. W., A. J. Watson, C. S. Law, E. R. Abraham, T. Trull, R. Murdoch, D. C. E. Bakker, A. R. Bowie, O. Buesseler, H. Chang, M. Charette, P. Croat, K. Downing, R. Frew, M. Gall, M. Hadfield, J. Hall, M. Harvey, G. Jameson, J. Laroche, M. Liddicoat, R. Ling, M. T. Maldonado, R. M. McKay, S. Nodder, S. Pickmere, R. Pridmore, S. Rintoul, K. Safi, P. Sutton, R. Strzepek, K. Tanneberger, S. Turner, A. Waite, and J. Zeldis. 2000. A mesoscale phytoplankton bloom

- in the polar Southern Ocean stimulated by iron fertilization. *Nature*, 407: 695–702.
- Bullard, J. E. 2013. Contemporary glacigenic inputs to the dust cycle. *Earth Surface Processes and Landforms*, 38:71–89.
- Cakmur, R. V., R. L. Miller, and O. Torres. 2004. Incorporating the effect of small scale circulations upon dust emission in an AGCM. *Journal of Geophysical Research*, 109:D07201.
- Capone, D. G., J. Zehr, H. Paerl, B. Bergman, and E. J. Carpenter. 1997. *Trichodesmium*: A globally significant marine cyanobacterium. *Science*, 276:1221–1229.
- Carroll, A. R., N. P. Stephens, M. S. Hendrix, and C. R. Glenn. 1998. Eolian-derived siltstone in the Upper Permian Phosphoria Formation: implications for marine upwelling. *Geology*, 26:1023–1026.
- Chadwick, O. A., L. A. Derry, P. M. Vitousek, B. J. Huebert, and L.O. Hedin. 1999. Changing sources of nutrients during four million years of ecosystem development. *Nature*, 397:491–497.
- Chen, J., G. Li, J. Yang, W. Rao, H. Lu, W. Balsam, Y. Sun, and J. Ji. 2007. Nd and Sr isotopic characteristics of Chinese deserts: implication for provenance of Asian dust. *Geochimica et Cosmochimica Acta*, 71:3904–3914.
- Coale, K. H., K. S. Johnson, S. E. Fitzwater, R. M. Gordon, S. Tanner, F. P. Chavez, L. Ferioli, C. Sakamoto, P. Rogers, F. Millero, P. Steinberg, P. Nightingale, D. Cooper, W. P. Cochlan, M. R. Landry, J. Constantinou, G. Rollwagen, A. Trasvina, and R. Kudela. 1996. A massive phytoplankton bloom induced by an ecosystem-scale iron fertilization experiment in the equatorial Pacific Ocean. *Nature*, 383:495–501.
- Conkright, M. E., S. Levitus, and T. P. Boyer. 1994. World Ocean Atlas 1994, Volume 1: Nutrients. NOAA Atlas NESDIS, 1.
- Cook, B. I., R. L. Miller, and R. Seager. 2008. Dust and sea surface temperature forcing of the 1930s “Dust Bowl” drought. *Geophysical Research Letters*, 35:L08710.
- Cook, B. I., R. L. Miller, and R. Seager. 2009. Amplification of the North American “Dust Bowl” drought through human-induced land degradation. *Proceedings of the National Academy of Sciences*, 106:4997.
- Cook, B. I., R. Seager, R. L. Miller, and J. A. Mason. 2013. Intensification of North American Megadroughts through surface and dust aerosol forcing. *Journal of Climate*, 26:4414–4430.
- Coude-Gaussen, G. 1987. The Perisaharan loess: sedimentological characterization and paleoclimatic significance. *GeoJournal*, 15:177–183.
- Crouvi, O., R. Amit, and Y. Enzel. 2010. Active sand seas and the formation of desert loess. *Quaternary Science Reviews*, 29:2087–2098.
- Crouvi, O., K. Schepanski, R. Amit, A. R. Gillespie, and Y. Enzel. 2012. Multiple dust sources in the Sahara Desert: The importance of sand dunes. *Geophysical Research Letters*, 39: L13401.
- Crowell, J. C. 1999. Pre-Mesozoic ice ages: their bearing on understanding the climate system. *Geological Society of America Memoir*, 192.
- Dahms, D. E. 1993. Mineralogical evidence for eolian contribution to soils of late Quaternary moraines, Wind River Mountains, Wyoming. *Geoderma*, 59:175–196.
- Davydov, V. I., J. L. Crowley, M. D. Schmitz, and V. I. Poletaev. 2010. High-precision U-Pb zircon age calibration of the global Carboniferous time scale and Milankovitch band cyclicity in the Donets Basin, eastern Ukraine. *Geochemistry, Geophysics, Geosystems*, 11:Q0AA04.
- Delmonte, B., C. Baroni, P. S. Andersson, H. Schonberg, M. Hansson, S. Aciego, J.-R. Petit, S. Albani, C. Mazziola, V. Maggi, and M. Frezzotti. 2010. Aeolian dust in the Talos Dome ice core (East Antarctica, Pacific/Ross Sea sector): Victoria Land versus remote sources over the last two climate cycles. *Journal of Quaternary Science*, 25:1327–1337.
- Demenocal, P. B., J. Ortiz, T. Guilderson, and M. Sarnthein. 2000. Coherent high- and low-latitude climate variability during the Holocene warm period. *Science*, 288: 2198–2202.
- Demott, P. J., K. Sassen, M. R. Poellot, D. Baumgardner, D. C. Rogers, S. D. Brooks, A. J. Prenni, and S. M. Kreidenweis. 2003. African dust aerosols as atmospheric ice nuclei. *Geophysical Research Letters*, 30:1732.
- DePaolo, D. J. 1980. Crustal growth and mantle evolution: inferences from models of element transport and Nd and Sr isotopes. *Geochimica et Cosmochimica Acta*, 44:1185–1196.
- DePaolo, W., and G. Wasserburg. 1976. Nd isotopic variations and petrogenetic models. *Geophysical Research Letters*, 3:249–252.
- DiMichele, W. A., and H. J. Falcon-Lang. 2011. Pennsylvanian ‘fossil forests’ in growth position ( $T^0$  assemblages): origin, taphonomic bias, and palaeoecological insights. *Journal of the Geological Society*, 168:585–605.
- Ding, Z. L., E. Derbyshire, S. L. Yang, Z. W. Yu, S. F. Xiong, and T. S. Liu. 2002. Stacked 2.6-Ma grain size record from the Chinese loess based on five sections and correlation with the deep-sea  $\delta^{18}\text{O}$  record. *Paleoceanography*, 17:1–21.
- Evans, J. E., and J. M. Reed. 2007. Integrated loessite-paleokarst depositional system, early Pennsylvanian Molas Formation, Paradox Basin, southwest Colorado, U.S.A. *Sedimentary Geology*, 195:161–181.
- Falcon-Lang, H. J. 2003. Late Carboniferous dryland tropical vegetation, Joggins, Nova Scotia, Canada.

- Palaios, 18:197–211.
- Falcon-Lang, H. J. 2006. Vegetation ecology of Early Pennsylvanian alluvial fan and piedmont environments in southern New Brunswick, Canada. *Palaeogeography, Palaeoclimatology, Palaeoecology*, 233:34–50.
- Fielding, C., T. Frank, and J. Isbell. 2008. The late Paleozoic ice age—a review of current understanding and synthesis of global climate patterns, p. 343–354. In C. R. Fielding, T. D. Frank, and J. I. Isbell (eds.), *Resolving the Late Paleozoic Ice Age in Time and Space*, Geological Society of America Special Paper, 441.
- Fischer, A. G., and M. Sarnthein. 1988. Airborne silts and dune-derived sands in the Permian of the Delaware Basin. *Journal of Sedimentary Petrology*, 58:637–643.
- Foster, T. M., G. S. Soreghan, M. J. Soreghan, K. C. Benison, and R. D. Elmore. 2014. Climatic and paleogeographic significance of eolian sediment in the Middle Permian Dog Creek Shale (Midcontinent U.S.). *Palaeogeography, Palaeoclimatology, Palaeoecology*, 402: 12–29.
- Gabbott, S., J. Zalasiewicz, R. Aldridge, and J. Theron. 2010. Eolian input into the Late Ordovician postglacial Soom Shale, South Africa. *Geology*, 38:1103–1106.
- Gallet, S., B. M. Jahn, B. Vanvliet Lanoe, A. Dia, and E. Rossello. 1998. Loess geochemistry and its implications for particle origin and composition of the upper continental crust. *Earth and Planetary Science Letters*, 156:157–172.
- Garrison, V. H., E. A. Shinn, W. T. Foreman, D. W. Griffin, C. W. Holmes, C. A. Kellogg, M. S. Majewski, L. L. Richardson, K. B. Ritchie, and G. W. Smith. 2003. African and Asian dust: from desert soils to coral reefs. *BioScience*, 53:469–480.
- Gerhart, L. M., and J. K. Ward. 2010. Plant responses to low CO<sub>2</sub> of the past. *New Phytologist*, 188:674–695.
- Giles, J. M., M. J. Soreghan, K. C. Benison, G. S. Soreghan, and S. T. Hasiotis. 2013. Lakes, loess, and paleosols in the Permian Wellington Formation of Oklahoma, U.S.A.: Implications for paleoclimate and paleogeography of the Midcontinent. *Journal of Sedimentary Research*, 83:825–846.
- Ginoux, P., M. Chin, I. Tegen, J. M. Prospero, B. Holben, O. Dubovik, and S.-J. Lin. 2001. Sources and distribution of dust aerosols simulated with the GOCART model. *Journal of Geophysical Research*, 106:20255–20273.
- Goebel, K. A., E. A. Bettis III, and P. H. Heckel. 1989. Upper Pennsylvanian paleosol in Stranger Shale and underlying Iatan Limestone, southwestern Iowa. *Journal of Sedimentary Petrology*, 59:224–232.
- Goldammer, R. K., E. J. Oswald, and P. A. Dunn. 1994. High-frequency glacio-eustatic cyclicity in the Middle Pennsylvanian of the Paradox Basin: an evaluation of Milankovitch forcing, p. 243–283. In P. L. de Boer and D. G. Smith (eds.), *Orbital Forcing and Cyclic Sequences*, International Association of Sedimentologists Special Publication 19, Blackwell Scientific.
- Grini, A., and C. S. Zender. 2004. Roles of saltation, sandblasting, and wind speed variability on mineral dust aerosol size distribution during the Puerto Rican Dust Experiment (PRIDE). *Journal of Geophysical Research*, 109:D07202.
- Grönvold, K., N. Óskarsson, S. J. Johnsen, H. B. Clausen, C. U. Hammer, G. Bond, and E. Bard. 1995. Ash layers from Iceland in the Greenland GRIP ice core correlated with oceanic and land sediments, *Earth and Planetary Science Letters*, 135:149–155.
- Groussset, F. E., and P. E. Biscaye. 2005. Tracing dust sources and transport patterns using Sr, Nd and Pb isotopes. *Chemical Geology*, 222:149–167.
- Gustavson, T. C., and V. T. Holliday. 1999. Eolian sedimentation and soil development on a semiarid to sub humid grassland, Tertiary Ogallala and Quaternary Blackwater Draw formations, Texas and New Mexico high plains. *Journal of Sedimentary Research*, 69:622–634.
- Goudie, A. S. 1983. Dust storms in space and time. *Progress in Physical Geography*, 7:502–530.
- Guo, Z. T., W. F. Ruddiman, Q. Z. Hao, H. B. Wu, Y. S. Qiao, R. X. Zhu, S. Z. Peng, J. J. Wei, B. Y. Yuan, and T. S. Liu. 2002. Onset of Asian desertification by 22 Myr ago inferred from loess deposits in China. *Nature*, 416:159–163.
- Hallock, P. and W. Schlager. 1986. Nutrient excess and the demise of coral reefs and carbonate platforms. *Palaios*, 1:389–398.
- Hamme, R. C., P. W. Webley, W. R. Crawford, F. A. Whitney, M. D. DeGrandpre, S. R. Emerson, C. C. Eriksen, K. E. Giesbrecht, J. F. Gower, and M. T. Kavanaugh. 2010. Volcanic ash fuels anomalous plankton bloom in subarctic northeast Pacific. *Geophysical Research Letters*, 37. doi: 10.1029/2010GL044629.
- Harrison, S. P., G. Yu, H. Takahara, and I. C. Prentice. 2001. Palaeovegetation (Communications arising). Diversity of temperate plants in east Asia. *Nature*, 413:129–130.
- Heavens, N. G., C. A. Shields, and N. M. Mahowald. 2012. A paleogeographic approach to aerosol prescription in simulations of deep time climate. *Journal of the Advances in the Modeling of Earth Systems*, 4:M11002.
- Heavens, N. G., N. M. Mahowald, G. S. Soreghan, M. J. Soreghan, and C. A. Shields. 2015. A model-based evaluation of tropical climate in Pangaea during the late Palaeozoic icehouse.

- Palaeogeography, Palaeoclimatology, Palaeoecology, 425:109–127.
- Highwood, E. J., and C. L. Ryder. 2014. Radiative effects of dust, p. 267–286. In P. Knippertz and J.-B. Stuut (eds.), *Mineral Dust: A Key Player in the Earth System*. Springer, Dordrecht.
- Hinnov, L. A. 2000. New perspectives on orbitally forced stratigraphy. *Annual Review of Earth and Planetary Sciences*, 28:419–475.
- Hinnov, L. A., and F. Hilgen. 2012. Chapter 4: Cyclostratigraphy and astrochronology, p. 63–83. In F. Gradstein, J. Ogg, G. Ogg, and D. Smith (eds.), *A Geologic Time Scale 2012*. Elsevier.
- Horton, D. E., C. J. Poulsen, and D. Pollard. 2010. Influence of high-latitude vegetation feedbacks on late Palaeozoic glacial cycles. *Nature Geoscience*, 3:572–577.
- Hovan, S. A., D. K. Rea, N. G. Pisias, and N. J. Shackleton. 1989. A direct link between the China Loess and marine  $\delta^{18}\text{O}$  records— aeolian flux to the North Pacific. *Nature*, 340:296–298.
- Jackson, J., M. Donovan, K. Cramer, and V. Lam. 2014. Status and trends of Caribbean coral reefs: 1970–2012. *Global Coral Reef Monitoring Network*, Washington, D.C.
- Jefferson, I. F., B. Q. Jefferson, A. M. Assallay, C. D. F. Rogers, and I. J. Smalley. 1997. Crushing of quartz sand to produce silt particles. *Naturwissenschaften*, 84: 148–149.
- Jiang, X., and W. R. Peltier. 1996. Ten million year histories of obliquity and precession: the influence of the ice-age cycle. *Earth and Planetary Science Letters*, 139:17–32.
- Jickells, T. D., Z. S. An, K. K. Andersen, A. R. Baker, G. Bergametti, N. Brooks, J. J. Cao, P. W. Boyd, R. A. Duce, K. A. Hunter, H. Kawahata, N. Kubilay, J. laRoche, P. S. Liss, N. Mahowald, J. M. Prospero, A. J. Ridgwell, I. Tegen, and R. Torres. 2005. Global iron connections between desert dust, ocean biogeochemistry, and climate. *Science*, 308:67–71.
- Johnson, S. Y. 1989. Significance of loessite in the Maroon Formation (Middle Pennsylvanian to Lower Permian), Eagle Basin, northwestern Colorado. *Journal of Sedimentary Petrology*, 59:782–791.
- Joussaume, S. 1993. Paleoclimatic tracers: An investigation using an atmospheric general circulation model under ice age conditions: 1 desert dust. *Journal of Geophysical Research*, 98:2767–2805.
- Kanayama, S., S. Yabuki, F. Yanagisawa, and R. Motoyama. 2002. The chemical and strontium isotope composition of atmospheric aerosols over Japan: the contribution of long-range-transported Asian dust (Kosa). *Atmospheric Environment*, 36:5159–5175.
- Kaplan, J. O., N. H. Bigelow, I. C. Prentice, S. P. Harrison, P. J. Bartlein, T. R. Christensen, W. Cramer, N. V. Matveyeva, A. D. McGuire, D. F. Murray, V. Y. Razzhivin, B. Smith, D. A. Walker, P. M. Anderson, A. A. Andreev, L. B. Brubaker, M. E. Edwards, and A. V. Lozhkin. 2003. Climate change and Arctic ecosystems: 2. Modeling, paleodate-model comparisons, and future projections. *Journal of Geophysical Research*, 108:8171.
- Kessler, J., G. Soreghan, and H. Wacker. 2001. Equatorial aridity in western Pangea: Lower Permian loessite and dolomitic paleosols in Northeastern New Mexico, USA. *Journal of Sedimentary Research*, 71:817–832.
- Kidron, G. J., M. Zohar, and A. Starinsky. 2014. Spatial distribution of dust deposition within a small drainage basin: Implications for loess deposits in the Negev Desert. *Sedimentology*, 61:1908–1922.
- Kiehl, J. T., and C. A. Shields. 2005. Climate simulation of the latest Permian: implications for mass extinction. *Geology*, 33:757–760.
- Kiessling, W. 2001. Paleoclimatic significance of Phanerozoic reefs. *Geology*, 29:751–754.
- Kiessling, W. 2009. Geologic and biologic controls on the evolution of reefs. *Annual review of ecology, evolution, and systematics*, 40:173–192.
- Kiessling, W., E. Flügel, and J. Golonka. 1999. Paleoreef maps: evaluation of a comprehensive database on Phanerozoic reefs. *AAPG Bulletin*, 83:1552–1587.
- Kodama, K. P., and L. A. Hinnov. 2015. *Rock Magnetic Cyclostratigraphy*. Wiley-Blackwell, Chichester, England.
- Kohfeld, K. E., K. C. Le Qu, S. P. Harrison, and R. F. Anderson. 2005. Role of marine biology in glacial-interglacial CO<sub>2</sub> cycles. *Science*, 308:74–78.
- Kok, J. F. 2011. A scaling theory for the size distribution of emitted dust aerosols suggests climate models underestimate the size of the global dust cycle. *Proceedings of the National Academy of Sciences of the United States of America*, 108:1016–1021.
- Kuenen, P. H. 1969. Origin of quartz silt. *Journal of Sedimentary Petrology*, 39:1631–1633.
- Kumar, R., I. F. Jefferson, K. O’Hara-Dhand, and I. J. Smalley. 2006. Controls on quartz silt formation by crystalline defects. *Naturwissenschaften*, 93:185–188.
- Kukla, G. 1987. Loess stratigraphy in central China. *Quaternary Science Reviews*, 6:191–219.
- Kukla, G., F. Heller, X. M. Liu, T. C. Xu, T. S. Liu, and Z. S. An. 1988. Pleistocene climates in China dated by magnetic susceptibility. *Geology*, 16:811–814.
- Kumar, N., R. F. Anderson, R. A. Mortlock, P. N. Froelich, P. L. Kunik, B. Dittrich-Hannen, and M. Suter. 1995. Increased biological productivity and

- export production in the glacial Southern Ocean. *Nature*, 378:675–680.
- Kurosaki, Y., M. Shinoda, and M. Mikami. 2011. What caused a recent increase in dust outbreaks over East Asia? *Geophysical Research Letters*, 38:L11702.
- Kutzbach, J. E., and R. G. Gallimore. 1989. Pangaean climates: megamonsoons of the megacontinent. *Journal of Geophysical Research*, 94:3341–3357.
- Lambeck, K., H. Rouby, A. Purcell, Y. Sun, and M. Sambridge. 2014. Sea level and global ice volume from the Last Glacial Maximum to the Holocene. *Proceedings of the National Academy of Sciences of the United States of America*, 111:15296–15303.
- Lapen, T. J., N. J. Mahlen, C. M. Johnson, and B. L. Beard. 2004. High precision Lu and Hf isotope analyses of both spiked and unspiked samples: a new approach. *Geochemistry Geophysics Geosystems*, 5:1.
- Laskar, J. 2013. Is the Solar System stable? *Progress in Mathematical Physics*, 66:239–270.
- Laskar, J., M. Gastineau, J.-B. Delisle, A. Farres And A. Fienga. 2011b. Strong chaos induced by close encounters with Ceres and Vesta. *Astronomy and Astrophysics*, 532:L4.
- Laskar, J., A. Fienga, M. Gastineau and H. Manche. 2011a. La2010: a new orbital solution for the long-term motions of the Earth. *Astronomy and Astrophysics*, 532:A89.
- Laskar, J., P. Robutel, F. Joutel, M. Gastineau, A. C. M. Correia, and B. Levrard. 2004. A long-term numerical solution for the insolation quantities of the Earth. *Astronomy and Astrophysics*, 428:261–285.
- Li, F., V. Ramaswamy, P. Ginoux, A. J. Broccoli, T. Delworth, and F. Zeng. 2010. Toward understanding the dust deposition in Antarctica during the Last Glacial Maximum: Sensitivity studies on plausible causes. *Journal of Geophysical Research*, 115:D24120.
- Luo, C., N. Mahowald, T. Bond, P. Y. Chuang, P. Artaxo, R. Siefert, Y. Chen, and J. Schauer. 2008. Combustion iron distribution and deposition. *Global Biogeochemical Cycles*, 22:GB1012.
- Lupker, M., S. M. Aciego, B. Bourdon, J. Schwander, and T. F. Stocker. 2010. Isotopic tracing (Sr, Nd, U and Hf) of continental and marine aerosols in an 18th century section of the Dye-3 ice core (Greenland). *Earth and Planetary Science Letters*, 295:277–286.
- Mack, G. H., and P. A. Dinterman. 2002. Depositional environments and paleogeography of the Lower Permian (Leonardian) Yeso and correlative formations in New Mexico. *The Mountain Geologist*, 39:75–88.
- Maher, B. A., and R. Thompson. 1991. Mineral magnetic record of the Chinese loess and paleosols. *Geology*, 19:3–6.
- Maher, B. A., and R. Thompson. 1995. Paleorainfall reconstructions from pedogenic magnetic susceptibility variations in the Chinese loess and paleosols. *Quaternary Research*, 44:383–391.
- Maher, B. A., J. M. Prospero, D. Mackie, D. Gaiero, P. P. Hesse, and Y. Balkanski. 2010. Global connections between aeolian dust, climate and ocean biogeochemistry at the present day and at the last glacial maximum. *Earth Science Reviews*, 99:61–97.
- Mahlen, N. J., B. L. Beard, C. M. Johnson, and T. J. Lapen. 2008. An investigation of dissolution methods for Lu-Hf and Sm-Nd isotope studies in zircon-and garnet-bearing whole-rock samples. *Geochemistry, Geophysics, Geosystems*, 9:1.
- Mahowald, N. 2011. Aerosol indirect effect on biogeochemical cycles and climate. *Science*, 334:794–796.
- Mahowald, N. M., and L. M. Kiehl. 2003. Mineral aerosol and cloud interactions. *Geophysical Research Letters*, 30:1475.
- Mahowald, N. M., K. Kohfeld, M. Hansson, Y. Balkanski, S. P. Harrison, I. C. Prentice, M. Schulz, and H. Rodhe. 1999. Dust sources and deposition during the last glacial maximum and current climate: A comparison of model results with paleodata from ice cores and marine sediments. *Journal of Geophysical Research*, 104: 15895–15916.
- Mahowald, N. M., D. R. Muhs, S. Levis, P. J. Rasch, M. Yoshioka, C. S. Zender, and C. Luo. 2006a. Change in atmospheric mineral aerosols in response to climate: Last glacial period, preindustrial, modern, and doubled carbon dioxide climates. *Journal of Geophysical Research*, 111:D10202.
- Mahowald, N. M., M. Yoshioka, W. D. Collins, A. J. Conley, D. W. Fillmore, and D. B. Coleman. 2006b. Climate response and radiative forcing from mineral aerosols during the last glacial maximum, pre-industrial, current, and doubled-carbon dioxide climates. *Geophysical Research Letters*, 33:L20705.
- Mahowald, N. M., S. Kloster, S. Engelstaedter, J. K. Moore, S. Mukhopadhyay, J. R. McConnell, S. Albani, S. C. Doney, A. Bhattacharya, M. A. J. Curran, M. G. Flanner, F. M. Hoffman, D. M. Lawrence, K. Lindsay, P. A. Mayewski, J. Neff, D. Rothenberg, E. Thomas, P. E. Thornton, and C. S. Zender. 2010. Observed 20<sup>th</sup> century desert dust variability: impact on climate and biogeochemistry. *Atmospheric Chemistry and Physics*, 10:10875–10893.
- Mahowald, N., D. S. Ward, S. Kloster, M. G. Flanner, C. L. Heald, N. G. Heavens, T. Hester, J.-F. Lamarque, and P. Y. Chuang. 2011. Aerosol impacts on climate and biogeochemistry. *Annual*

- Review of Environmental Resources, 36:45–74.
- Marticorena, B., and G. Bergametti. 1995. Modeling the atmospheric dust cycle: 1. Design of a soil-derived emission scheme. *Journal of Geophysical Research*, 100:16415–16430.
- Martin, J. H., and S. E. Fitzwater. 1989. Iron deficiency limits phytoplankton growth in the north-east Pacific subarctic. *Nature*, 331:341–343.
- Martin, J. H. 1991. Iron still comes from above. *Nature*, 353:123.
- Martin, J. H., R. M. Gordon, and S. E. Fitzwater. 1991. The case for iron. *Limnology and Oceanography*, 36:1793–1802.
- Martin, J. H., K. H. Coale, K. S. Johnson, S. E. Fitzwater, R. M. Gordon, S. J. Tanner, C. N. Hunter, V. A. Elrod, J. L. Nowicki, T. L. Coley, R. T. Barber, S. Lindley, A. J. Watson, K. Van Scoy, C. S. Law, M. I. Liddicoat, R. Ling, T. Stanton, J. Stockel, C. Collins, A. Anderson, R. Bidigare, M. Ondrusek, M. Latasa, F. J. Millero, K. Lee, W. Yao, J. Z. Zhang, G. Friederich, C. Sakamoto, F. Chavez, K. Buck, Z. Kolber, R. Greene, P. Falkowski, S. W. Chisholm, F. Hoge, R. Swift, J. Yungel, S. Turner, P. Nightingale, A. Hatton, P. Liss, and N. W. Tindale. 1994. Testing the iron hypothesis in ecosystems of the equatorial Pacific Ocean. *Nature*, 371:123–129.
- Martin, R. V., D. J. Jacob, R. M. Yantosca, M. Chin, and P. Ginoux. 2003. Global and regional decreases in tropospheric oxidants from photochemical effects of aerosols. *Journal of Geophysical Research*, 108:4097.
- Mason, J., and P. Jacobs. 1998. Chemical and particle-size evidence for addition of fine dust to soils of the Midwestern United States. *Geology*, 26:1135–1138.
- Mason, J. A., E. A. Nater, C. W. Zanner, and J. C. Bell. 1999. A new model of topographic effects on the distribution of loess. *Geomorphology*, 28:223–236.
- Melvin, J., R. A. Sprague, and C. J. Heine. 2010. From bergs to ears: the Late Paleozoic Gondwanan glaciation and its aftermath in Saudi Arabia, p. 37–80. *In* O. R. López-Gamundi and L. A. Buatois (eds.), *Late Paleozoic Glacial Events and Postglacial Transgressions in Gondwana*, Geological Society of America Special Paper, 468.
- Meyers, S. R., and B. B. Sageman. 2007. Quantification of deep-time orbital forcing by Average Spectral Misfit. *American Journal of Science*, 307:773–792.
- Miller, R. L., P. Knippertz, C. P. Garcia-Pando, J. P. Perlitz, and I. Tegen. 2014. Impact of dust radiative forcing upon climate, p. 327–357. *In* P. Knippertz and J.-B. Stuut (eds.), *Mineral Dust: A Key Player in the Earth System*. Springer, Dordrecht.
- Montañez, I. P., N. J. Tabor, D. Niemeier, W. A. DiMichele, T. D. Frank, C. R. Fielding, J. L. Isbell, L. P. Birgenheier, and M.C. Rygel. 2007. CO<sub>2</sub>-forced climate and vegetation instability during late Paleozoic deglaciation. *Science*, 315:87–91.
- Moore, J. K., and S. C. Doney. 2007. Iron availability limits the ocean nitrogen inventory stabilizing feedbacks between marine denitrification and nitrogen fixation. *Global Biogeochemical Cycles*, 21:GB2001.
- Moore, C. M., M. M. Mills, A. Milne, R. Langlois, E. P. Achterberg, K. Lochte, R. J. Geider, and J. Laroche. 2006. Iron limits primary productivity during spring bloom development in the central North Atlantic. *Global Change Biology*, 12:626–634.
- Morche, W., H. W. Hubberten, A. Mackensen, and J. Keller. 1992. Geochemistry of Cenozoic ash layers from the Kerguelen Plateau (Leg 120): A first step toward a tephrostratigraphy of the southern Indian Ocean. *In* R. Schlich and S. W. Wise, Jr. (eds.), *Proceedings of the Ocean Drilling Program, Scientific Results, Volume 120*. doi: 10.2973.odp.proc.sr.120.163.1992
- Morley, R. J. 2011. Cretaceous and Tertiary climate change and the past distribution of megathermal rainforests, p. 1–34. *In* M. B. Bush, J. R. Flenley, and W. D. Gosling (eds.), *Tropical Rainforest Responses to Climatic Change* (Second Edition), Springer-Verlag, Berlin.
- Moxim, W. J., S.-M. Fan, and H. Levy II. 2011. The meteorological nature of variable solute transport and deposition within the North Atlantic Ocean basin. *Journal of Geophysical Research*, 116:D03203.
- Muhs, D. R. 2013. The geologic records of dust in the Quaternary. *Aeolian Research*, 9:3–48.
- Muhs, D. R., and E. A. Bettis III. 2003. Quaternary loess-paleosol sequences as an example of climatic extremes, p. 53–74. *In* M. A. Chan and A. W. Archer (eds.), *Extreme Depositional Environments: Mega End Members in Geologic Time*. Geological Society of America Special Publication, 370.
- Muhs, D. R., E. A. Bettis, J. N. Aleinikoff, J. P. McGeehin, J. Beann, G. Skipp, B. D. Marshall, H. M. Roberts, W. C. Johnson, and R. Benton. 2008. Origin and paleoclimatic significance of late Quaternary loess in Nebraska: Evidence from stratigraphy, chronology, sedimentology, and geochemistry. *Geological Society of America Bulletin*, 120: 1378–1407.
- Murphy, K. 1987. Eolian origin of upper Paleozoic red siltstones at Mexican Hat and Dark Canyon, southeastern Utah. Unpublished M.S. Thesis, University of Nebraska at Lincoln, 128 p.
- Nahon, D., and R. Trompette. 1982. Origin of siltstones: glacial grinding versus weathering.

- Sedimentology, 29:25–35.
- Newman, C. E., S. R. Lewis, P. L. Read, and F. Forget. 2002. Modeling the Martian dust cycle: 1. Representations of dust transport processes. *Journal of Geophysical Research*, 107:5123.
- Nichol, J. E., and D. W. Nichol. 2013. Pleistocene loess in the humid subtropical forest zone of East Asia. *Geophysical Research Letters*, 40:1978–1983.
- Nie, J., Y. Song, J. W. King, R. Zhang, and X. Fang. 2013. Six million years of magnetic grain-size records reveal that temperature and precipitation were decoupled on the Chinese Loess Plateau during ~4.5–2.6 Ma. *Quaternary Research*, 79:465–470.
- Nie, J., W. Peng, A. Möller, Y. Song, D. F. Stockli, T. Stevens, B. K. Horton, S. Liu, A. Bird, J. Oalmann, H. Gong, and X. Fang. 2014. Provenance of the upper Miocene–Pliocene Red Clay deposits of the Chinese loess plateau. *Earth and Planetary Science Letters*, 407:35–47.
- Okin, G. S. 2008. A new model of wind erosion in the presence of vegetation. *Journal of Geophysical Research*, 113:F02S10.
- Okin, G. S., and D. A. Gillette. 2001. Distribution of vegetation in wind-dominated landscapes: Implications for wind erosion modeling and landscape processes. *Journal of Geophysical Research*, 106:9673–9683.
- Okin, G. S., N. Mahowald, O. A. Chadwick, and P. Artaxo. 2004. Impact of desert dust on the biogeochemistry of phosphorus in terrestrial ecosystems. *Global Biogeochemical Cycles*, 18:GB2005.
- Okin, G. S., A. R. Baker, I. Tegen, N. M. Mahowald, F. J. Dentener, R. A. Duce, J. N. Galloway, K. Hunter, M. Kanakidou, N. Kubilay, J. M. Prospero, M. Sarin, V. Surapipith, M. Uematsu, and T. Zhu. 2011. Impacts of atmospheric nitrogen deposition on marine productivity: Roles of nitrogen, phosphorus, and iron. *Global Biogeochemical Cycles*, 25:GB2022.
- Pagani, M., K. Caldeira, R. Berner, and D. J. Beerling. 2009. The role of terrestrial plants in limiting atmospheric CO<sub>2</sub> decline over the past 24 million years. *Nature*, 460:85–88.
- Patchett, P. J., and M. Tatsumoto. 1980. Hafnium isotope variations in oceanic basalts. *Geophysical Research Letters*, 7:1077–1080.
- Patterson, E. M. 2011. Fluctuating dust in the late Paleozoic icehouse: Records from an oceanic atoll, Akiyoshi, Japan. Unpublished M.S. Thesis, University of Oklahoma, 115 p.
- Paytan, A., and K. McLaughlin. 2007. The oceanic phosphorus cycle. *Chemical Reviews*, 107:563–576.
- Peltier, W. R., D. F. Argus, and R. Drummond. 2015. Space geodesy constrains ice age terminal deglaciation: The global ICE-6G\_C (VM5a) model. *Journal of Geophysical Research Solid Earth*, 120:450–487.
- Peyser, C. E., and C. J. Poulsen. 2008. Controls on Permo–Carboniferous precipitation over tropical Pangaea: a GCM sensitivity study. *Palaeogeography, Palaeoclimatology, Palaeoecology*, 268:181–192.
- Pickett, E. J., S. P. Harrison, G. Hope, K. Harle, J. R. Dodson, A. P. Kershaw, I. C. Prentice, J. Backhouse, E. A. Colhoun, D. D’costa, J. Flenley, J. Grindrod, S. Haberle, C. Hassell, C. Kenyon, M. Macphail, H. Martin, A.H. Martin, M. Mckenzie, J.C. Newsome, D. Penny, J. Powell, J. I. Raine, W. Southern, J. Stevenson, J.-P. Sutra, I. Thomas, S. Van Der Kaars, and J. Ward. 2004. Pollen-based reconstructions of biome distributions for Australia, Southeast Asia, and the Pacific (SEAPAC region) at 0, 6000, and 18000 <sup>14</sup>C yr BP. *Journal of Biogeography*, 31:1381–1444.
- Porter, S. C., and Z. An. 1995. Correlation between climate events in the North Atlantic and China during the last glaciation. *Nature*, 375:305–308.
- Porter, S. C. 2001. Chinese loess record of monsoon climate during the last glacial-interglacial cycle. *Earth-Science Reviews*, 54:115–128.
- Prasad, V., C. A. E. Strömberg, H. Alimohammadian, and A. Sahni 2005. Dinosaur coprolites and the early evolution of grasses and grazers. *Science*, 310:1177–1180.
- Prentice, I. C., D. Jolly, and Biome 6000 Participants. 2000. Mid-Holocene and glacial-maximum vegetation geography of the northern continents and Africa. *Journal of Biogeography*, 27:507–519.
- Prospero, J. P., J. E. Bullard, and R. Hodgkins. 2012. High latitude dust over the North Atlantic: inputs from Icelandic proglacial dust storms. *Science*, 335: 1078–1082.
- Prospero, J. P., P. Ginoux, O. Torres, S. E. Nicholson, and T. E. Gill. 2002. Environmental characterisation of global sources of atmospheric soil dust identified with the Nimbus 7 Total Ozone Mapping Spectrometer (TOMS) absorbing aerosol product. *Reviews of Geophysics*, 40: 21–31.
- Pullen, A., P. Kapp, A. T. McCallister, H. Chang, G. E. Gehrels, C. N. Garzjone, and R.V. Heermance. 2011. Qaidam Basin and northern Tibetan Plateau as dust sources for the Chinese Loess Plateau and paleoclimatic implications. *Geology*, 39:1031–1034.
- Pye, K. 1987. Aeolian Dust and Dust Deposits. Academic Press, London.
- Pye, K. 1989. Processes of fine particle formation, dust source regions, and climatic changes, p. 3–30. In M. Leinen and M. Sarnthein (eds.), *Paleoclimatology and Paleometeorology: Modern and Past Patterns of Global Atmospheric Transport*, Kluwer Academic Publishers,

- Dordrecht, The Netherlands.
- Pye, K. 1995. The nature, origin, and accumulation of loess. *Quaternary Science Review*, 14:653–667.
- Pye, K., and D. Sherwin. 1999. Loess, p. 213–238. In A. S. Goudie, I. Livingstone, and S. Stokes (eds.), *Aeolian Environments, Sediments, and Landforms*. John Wiley & Sons, Chichester, United Kingdom.
- Rea, D. K. 1994. The paleoclimatic record provided by eolian deposition in the deep-sea—The geologic history of wind. *Reviews of Geophysics*, 32:159–195.
- Rees, P. M., A. M. Ziegler, M. T. Gibbs, J. E. Kutzbach, P. J. Behling, and D. B. Rowley. 2002. Permian phytogeographic patterns and climate data/model comparisons. *The Journal of Geology*, 110:1–31.
- Retallack, G. J. 1982. Paleopedological perspectives on the development of grasslands during the Tertiary. *Proceedings of Third North American Paleontological Convention*, 2:417–421.
- Retallack, G. J. 1992. Paleozoic paleosols, p. 543–654. In P. Martini (ed.), *Weathering, Soil, and Paleosols*. Elsevier, Amsterdam.
- Rickli, J., M. Frank, A. R. Baker, S. M. Aciego, G. de Souza, R. B. Georg, and A. N. Halliday. 2010. Hafnium and neodymium isotopes in surface waters of the eastern Atlantic Ocean: Implications for sources and inputs of trace metals to the ocean. *Geochimica et Cosmochimica Acta*, 74:540–557.
- Ridgwell, A. 2002. Dust in the Earth system: The biogeochemical linking of land, air, and sea. *Philosophical Transactions of the Royal Society of London*, 360:1–21.
- Ridley, D. A., C. L. Heald, J. R. Pierce, and M. J. Evans. 2013. Toward resolution-independent dust emissions in global models: Impacts on the seasonal and spatial distribution of dust. *Geophysical Research Letters*, 40:2873–2877.
- Riggs, N. R., T. M. Lehman, G. E. Gehrels, and W. R. Dickinson. 1996. Detrital zircon link between headwaters and terminus of the Upper Triassic Chinle-Dockum paleoriver system. *Science*, 273:97–100.
- Rosenfeld, D., Y. Rudich, and R. Lahav. 2001. Dust suppressing precipitation: A possible desertification feedback loop. *Proceedings of the National Academy of Sciences of the United States of America*, 98: 5975–5980.
- Ruth, U., D. Wagenbach, J. P. Steffensen, and M. Bigler. 2003. Continuous record of microparticle concentration and size distribution in the central Greenland NGRIP ice core during the last glacial period. *Journal of Geophysical Research*, 108:4098.
- Sageman, B., and T. Lyons. 2004. Geochemistry of fine-grained sediments and sedimentary rocks. *Treatise on Geochemistry*, 7:116–158.
- Sarnthein, M., G. Tetzlaff, B. Koopmann, K. Wolter, and U. Pflaumann. 1981. Glacial and interglacial wind regimes over the astern subtropical Atlantic and North-West Africa. *Nature*, 293:193–196.
- Scotese, C. R. 2001. *Atlas of Earth history*. PALEOMAP Project of the University of Texas at Arlington, Arlington, TX.
- Schmitz, M. D., and V. I. Davydov. 2012. Quantitative radiometric and biostratigraphic calibration of the Pennsylvanian-Early Permian (Cisuralian) time scale and pan-Euramerican chronostratigraphic correlation. *Geological Society of America Bulletin*, 124:549–577.
- Shao, Y. 2008. *Physics and Modelling of Wind Erosion*. Springer-Verlag, Berlin.
- Shinn, E. A., G. W. Smith, J. M. Prospero, P. Betzer, M. L. Hayes, V. Garrison, and R. T. Barber. 2000. African dust and the demise of Caribbean coral reefs. *Geophysical Research Letters*, 27:3029–3032.
- Slomp, C. P., and P. Van Cappellen. 2004. Nutrient inputs to the coastal ocean through submarine groundwater discharge: controls and potential impact. *Journal of Hydrology*, 295:64–86.
- Smalley, I. J. 1966. The properties of glacial loess and the formation of loess deposits. *Journal of Sedimentary Petrology*, 36:669–676.
- Smalley, I. J. 1990. Possible formation mechanisms for the modal coarse silt quartz particles in loess. *Quaternary International*, 7–8:23–27.
- Smalley, I. J. 1995. Making the material; the formation of silt-sized primary mineral particles for loess deposits. *Quaternary Science Reviews*, 14:645–651.
- Smalley, I., K. O'Hara-Dhand, J. Wint, B. Machalett, Z. Jary, and I. Jefferson. 2009. Rivers and loess: The significance of long river transportation in the complex event-sequence approach to loess deposit formation. *Quaternary International*, 198:7–18.
- Smith, S. V. 1984. Phosphorous versus nitrogen limitation in the marine environment: Limnology and Oceanography, 29:1149–1160.
- Soreghan, G. S. 1992. Preservation and paleoclimatic significance of eolian dust in the Ancestral Rocky Mountains province. *Geology*, 20:1111–1114.
- Soreghan, G. S., and M. J. Soreghan. 2002. Atmospheric dust and algal dominance in the Late Paleozoic: A hypothesis. *Journal of Sedimentary Research*, 72:457–461.
- Soreghan, G. S., and A. S. Cohen. 2013. Scientific drilling and the evolution of the earth system: climate, biota, biogeochemistry, and extreme events. *Scientific Drilling*, 16:63–72.
- Soreghan, G. S., R. D. Elmore, B. Katz, M. Cogoini, and S. Banerjee. 1997. Pedogenically enhanced magnetic susceptibility variations preserved in Paleozoic loessite: *Geology*, 25:1003–1006.
- Soreghan, G. S., R. D. Elmore, and M. Lewchuk. 2002.

- Sedimentologic-magnetic record of western Pangean climate in upper Paleozoic loessite (lower Cutler beds, Utah). *Bulletin of the Geological Society of America*, 114:1019–1035.
- Soreghan, G. S., A. M. Moses, M. J. Soreghan, M. A. Hamilton, C. M. Fanning, and P. K. Link. 2007. Palaeoclimatic inferences from upper Palaeozoic siltstone of the Earp Formation and equivalents, Arizona–New Mexico (USA). *Sedimentology*, 54:701–719.
- Soreghan, G. S., M. J. Soreghan, and M. A. Hamilton. 2008. Origin and significance of loess in late Paleozoic western Pangaea: A record of tropical cold?. *Palaeogeography, Palaeoclimatology, Palaeoecology*, 268:234–259.
- Soreghan, G. S., N. Heavens, E. P. Patterson, H. Sano, N. Mahowald, V. Davydov, and M. J. Soreghan. 2011. Giant grains from Pennsylvanian dust of the Panthalassic Ocean: Evidence for extreme winds and a Paleo-Tethyan monsoon. *AGU Fall Meeting Abstracts*, Abstract PP22D-07.
- Soreghan, G. S., Y. J. Joo, M. E. E. Madden, and S. C. Van Deventer. 2015. Silt production as a function of climate and lithology under simulated comminution. *Quaternary International*, 1–10. doi: 10.1016/j.quaint.2015.05.010
- Soreghan, M. J., G. S. Soreghan, and M. A. Hamilton. 2002. Paleowinds inferred from detrital-zircon geochronology of upper Paleozoic loessite, western equatorial Pangaea. *Geology*, 30:695–698.
- Soreghan, M. J., and P. Francus. 2004. Processing backscattered electron digital images of thin sections, p. 203–225. In P. Francus (ed.), *Image Analysis, Sediments and Paleoenvironments*. Kluwer Academic Publishers, Dordrecht, The Netherlands.
- Soreghan, M. J., and G. S. Soreghan. 2007. Whole-rock geochemistry of upper Paleozoic loessite, western Pangaea: Implications for paleo-atmospheric circulation. *Earth and Planetary Science Letters*, 255:117–132.
- Soreghan, M. J., G. S. Soreghan, and M. A. Hamilton. 2008. Glacial-interglacial shifts in atmospheric circulation of western tropical Pangaea. *Palaeogeography, Palaeoclimatology, Palaeoecology*, 268:260–272.
- Soreghan, M. J., N. Heavens, G. S. Soreghan, P. K. Link, and M. A. Hamilton. 2014. Abrupt and high-magnitude changes in atmospheric circulation recorded in the Permian Maroon Formation, tropical Pangaea. *Geological Society of America Bulletin*, 126: 569–584.
- Stevens, T., C. Palk, A. Carter, H. Lu, and P. D. Clift 2010. Assessing the provenance of loess and desert sediments in northern China using U-Pb dating and morphology of detrital zircons. *Geological Society of America Bulletin*, 122:1331–1344.
- Stuut, J.-B., M. Zabel, V. Ratmeyer, P. Helmke, E. Schefuss, G. Lavik, and R. Schneider. 2005. Provenance of present-day eolian dust collected off NW Africa. *Journal of Geophysical Research*, 110:D04202.
- Sun, D. H. J. Shaw, Z. S. An, M. Y. Cheng, and L. P. Yue. 1998. Magnetostratigraphy and paleoclimatic interpretation of continuous 7.2 Ma late Cenozoic aeolian sediments from the Chinese Loess Plateau. *Geophysical Research Letters*, 25:85–88.
- Sun, J. 2002. Provenance of loess material and formation of loess deposits on the Chinese Loess Plateau. *Earth and Planetary Science Letters*, 203:845–859.
- Sun, Y., H. Lu, and Z. An. 2006. Grain size of loess, palaeosol and Red Clay deposits on the Chinese Loess Plateau: Significance for understanding pedogenic alteration and palaeomonsoon evolution. *Palaeogeography, Palaeoclimatology, Palaeoecology*, 241: 129–138.
- Sur, S., G. Soreghan, M. Soreghan, W. Yang, and A. Saller. 2010a. A record of glacial aridity and Milankovitch-scale fluctuations in atmospheric dust from the Pennsylvanian tropics. *Journal of Sedimentary Research*, 80:1046–1067.
- Sur, S., M. J. Soreghan, G. S. Soreghan, and A. F. Stagner. 2010b. Extracting the silicate mineral fraction from ancient carbonate: assessing the geologic record of dust. *Journal of Sedimentary Research*, 80:763–769.
- Sweeney, M. R., and J. A. Mason. 2013. Mechanisms of dust emission from Pleistocene loess deposits, Nebraska, USA. *Journal of Geophysical Research Solid Earth*, 118:1460–1471.
- Sweeney, M. R., E. V. McDonald, and V. Etyemezian. 2011. Quantifying dust emissions from desert landforms, eastern Mojave Desert, USA. *Geomorphology*, 135:21–34.
- Sweet, A. C., G. S. Soreghan, D. E. Sweet, M. J. Soreghan, and A. S. Madden. 2013. Permian dust in Oklahoma: Source and origin for Middle Permian (Flowerpot-Blaine) redbeds in Western Tropical Pangaea. *Sedimentary Geology*, 284–285:181–196.
- Taner, M. T. 2000. *Attributes Revisited*. Technical Publication, Rock Solid Images, Inc., Houston, Texas.
- Tegen, I., A. A. Lacis, and I. Fund. 1996. The influence on climate forcing of mineral aerosols from disturbed soils. *Nature*, 380:419–422.
- Tegen, I., S. P. Harrison, K. E. Kohfeld, and M. Werner. 2001. Dust deposition and aerosols in the last glacial maximum and their climate effects. *Nova Acta Leopoldina*, 88:71–78.
- Thomson, D. J. 1990. Quadratic inverse spectrum estimates: Applications to paleoclimatology. *Philosophical Transactions of the Royal Society of London, Series A*, 332:539–597.

- Thomson, D. J. 1982. Spectrum estimation and harmonic analysis. Proceedings of the IEEE, 70:1055–1096.
- Tramp, K. L., G. S. Soreghan, and R. D. Elmore. 2004. Paleoclimatic inferences from paleopedology and magnetism of the Permian Maroon Formation loessite, Colorado, USA. Geological Society of America Bulletin, 116:671–686.
- TSCreator visualization of enhanced Geologic Time Scale 2012 database (Version 6.3; 2015) James Ogg (database coordinator) and Adam Lugowski (software developer) <http://www.tscreator.org>
- Warren, A., A. Chappell, M. C. Todd, C. S. Bristow, N. Drake, S. Engelstaedter, V. Martins, S. M'bainayel, and R. Washington. 2007. Dust-raising in the dustiest place on earth. Geomorphology, 92: 25–37.
- Washington, R., M. C. Todd, G. Lizcano, I. Tegen, C. Flamant, I. Koren, P. Ginoux, S. Engelstaedter, C. S. Bristow, C. S. Zender, A. S. Goudie, and J. M. Prospero. 2006. Links between topography, wind, deflation, lakes and dust: the case of the Bodele Depression, Chad. Geophysical Research Letters, 33: L09401.
- Watkins, R., and E. C. Wilson. 1989. Paleoecologic and biogeographic significance of the biostromal organism *Palaeoaplysina* in the Lower Permian McCloud Limestone, eastern Klamath Mountains, California. Palaios, 4:181–192.
- Weaver, J. E., and G. W. Harmon. 1935. Quantity of living plant materials in prairie soil in relation to run-off and soil erosion. Conservation Department of the Conservation and Survey Division of the University of Nebraska Bulletin, 8, 53 p.
- Williams, G., 2000. Geological constraints on the Precambrian history of Earth's rotation and the Moon's orbit. Reviews of Geophysics, 38:37–59.
- Wilson, J. P., and A. H. Knoll. 2010. A physiologically explicit morphospace for tracheid-based water transport in modern and extinct seed plants. Paleobiology, 36:335–355.
- Wright, J., B. Smith, and B. Whalley. 1998. Mechanisms of loess-sized quartz silt production and their relative effectiveness: laboratory simulations. Geomorphology, 23:15–34.
- Wright, J. S. 2001. Making loess-sized quartz silt: data from laboratory simulations and implications for sediment transport pathways and the formation of “desert” loess deposits associated with the Sahara. Quaternary International, 76–77:7–19.
- Yaalon, D. H. 1974. Accumulation and distribution of loess-derived deposits in the semi-desert and desert fringe areas of Israel. Geomorphology, 20: 91–105.
- Yaalon, D. H., and E. Ganor. 1973. The influence of dust on soils in the Quaternary. Soil Science, 116:146–155.
- Yao, X., Y. Zhou, and L. A. Hinnov. 2015. Astronomical forcing of Middle Permian chert in the Lower Yangtze area, South China. Earth and Planetary Science Letters, 422:206–221.
- Yeager, S. G., C. A. Shields, W. G. Large, and J. J. Hack. 2006. The low-resolution CCSM3. Journal of Climate, 19:2545–2566.
- Yoshioka, M., N. M. Mahowald, A. J. Conley, W. D. Collins, D. W. Fillmore, C. S. Zender, and D. B. Coleman. 2007. Impact of desert dust radiative forcing on Sahel precipitation: relative importance of dust compared to sea surface temperature variations, vegetation changes, and greenhouse gas warming. Journal of Climate, 20:1445–1467.
- Zender, C. S., H. Bian, and D. Newman. 2003a. Mineral Dust Entrainment and Deposition (DEAD) model: Description and 1990s dust climatology. Journal of Geophysical Research, 108:4416.
- Zender, C. S., D. Newman, and O. Torres. 2003. Spatial heterogeneity in aeolian erodibility: uniform, topographic, geomorphic, and hydrologic hypotheses. Journal of Geophysical Research, 108:4543.
- Ziegler, A. M., M. J. Hulver, and D. B. Rowley. 1997. Permian world topography and climate, p. 111–146. In L. P. Martini (ed.), Late Glacial and Postglacial Environmental Changes: Quaternary, Carboniferous–Permian, and Proterozoic. Oxford University Press, Oxford, United Kingdom.